DOT/FAA/TC-15/47

Federal Aviation Administration
William J. Hughes Technical Center
Aviation Research Division
Atlantic City International Airport
New Jersey 08405

Teardown Evaluation of a Composite Carbon/Epoxy Beechcraft Starship Aft Wing

September 2017

Final Report

U.S. Department of Transportation
Federal Aviation Administration

NOTICE

Technical Report Documentation Page

1. Report No.	2. Government Accession No.	3. Recipient's Catalog No.
DOT/FAA/TC-15/47		

4. Title and Subtitle	5. Report Date
TEARDOWN EVALUATION OF A COMPOSITE CARBON/EPOXY BEECHCRAFT STARSHIP AFT WING	September 2017
	6. Performing Organization Code

7. Author(s)	8. Performing Organization Report No.
John S. Tomblin and Lamia Salah	

9. Performing Organization Name and Address	10. Work Unit No. (TRAIS)
National Institute for Aviation Research Wichita State University Wichita, KS 67260	
	11. Contract or Grant No.

12. Sponsoring Agency Name and Address	13. Type of Report and Period Covered
FAA Northwest Mountain Regional Office 1601 Lind Avenue SW Renton, WA 98057	Final Report
	14. Sponsoring Agency Code AIR-100

15. Supplementary Notes

The FAA William J. Hughes Technical Center Aviation Research Division COR was Curtis Davies.

16. Abstract

This report summarizes the findings of a study conducted on a composite carbon/epoxy Beechcraft Starship aft wing to determine the effects of aging after 12 years of service and 1800 flight hours. The Beechcraft Starship was the world's first pressurized all-composite business turboprop and received Federal Aviation Administration certification in 1987. Only 53 Starships were manufactured; production was discontinued because of poor demand. Because of economic reasons and prohibitive fleet support costs, the original equipment manufacturer gathered and destroyed most of its Starship fleet.

This report provides highlights of the results of the teardown study conducted on a Starship NC-8 aft wing. Results indicated that the composite structure maintained its structural integrity over 1800 flight hours with no significant degradation or detrimental signs of aging observed. It should be noted that the number of flight hours was too small to integrate the effects of mechanical fatigue.

17. Key Words	18. Distribution Statement
Beechcraft Starship; Carbon/epoxy; Aging composites	This document is available to the U.S. public through the National Technical Information Service (NTIS), Springfield, Virginia 22161. This document is also available from the Federal Aviation Administration William J. Hughes Technical Center at actlibrary.tc.faa.gov.

19. Security Classif. (of this report)	20. Security Classif. (of this page)	21. No. of Pages	22. Price
Unclassified	Unclassified	47	

ACKNOWLEDGMENTS

The authors would like to thank Ric Abbott for his invaluable input to the program. The authors also thank Tim Hickey, Abhijit Sonambekar, John Fitzpatrick, Antony Alford, Ping Taoh, and Chathuranga Kuruppuarachchige from the National Institute for Aviation Research.

TABLE OF CONTENTS

		Page
EXECUTIVE SUMMARY		ix
1.	INTRODUCTION	1
2.	BEECHCRAFT STARSHIP AFT WING TEARDOWN STUDY	1
2.1	Test Article Description	1
2.2	Material Selection	5
2.3	Lightning Protection Scheme	5
2.4	Supporting Data for Certification	6
2.5	Left Wing-section NDi	6
2.6	Thermal Analysis	7
2.7	Moisture Content Evaluation	21
2.8	Microscopy	22
2.9	Starship Aft Wing Full-Scale Test	26
2.9.1	Full-Scale Article—NDI	26
2.9.2	Starship Aft Wing Full-Scale Test	29
3.	CONCLUSIONS	36
4.	REFERENCES	37

LIST OF FIGURES

Figure		Page
1	Beechcraft Starship under investigation (NC-8)	2
2	Beechcraft Starship airplane 3-view drawing with dimensions	3
3	Beechcraft Starship aft wing structural details	4
4	The (a) Starship aft wing structural H-joint details and (b) H-joint extracted from BL78 upper skin center spar	5
5	The (a) Starship aft wing structural V-joint details and (b) V-joint extracted from BL78 lower skin front spar	5
6	Beechcraft Starship aft wing TTU scans of the left upper- and lower-wing skins	7
7	Aft wing coupon nomenclature	8
8	DMA results for sample extracted from LS BL208 UF16 FS450	9
9	DMA results for sample extracted from LS BL48 UF35 FS402	9
10	DMA results for coupons extracted from NC-8 aft wing LS	11
11	DMA results for a sample extracted from US BL50 LF25 FS369	12
12	DMA results for a sample extracted from US BL74 LF25 FS369	12
13	DMA results for a sample extracted from US BL259 UF5 FS459	13
14	DMA results for coupons extracted from NC-8 aft wing US	15
15	DSC data for a sample extracted from LS BL50 LF28 FS 394	16
16	DSC data for a sample extracted from LS BL48 UF38 FS405	16
17	DSC data for a sample extracted from LS BL260 UF7 FS461	17
18	DSC data for a sample extracted from US BL50 LF27 FS 371	19
19	DSC data for a sample extracted from US BL74 LF17 FS 371	19
20	Moisture loss as function of time for coupons extracted from LS	21
21	Moisture loss as a function of time for coupons extracted from the US	22
22	US BL48 UF 39	23
23	US BL48 UF 40	23
24	US BL140 UF 20	24
25	US BL140 UF 19	24
26	US BL140 LF 19	25
27	US BL140 LF 20	25
28	LS BL74 LF 29	25

29	LS BL208 UF 20	26
30	Overview of the right upper aft wing of the Starship	27
31	Overview of the right lower aft wing of the Starship	28
32	Aft wing repair of US area 7 damage	29
33	Full-scale test setup	30
34	Bending moment vs. LSTA	31
35	Starship right main wing strain gage identification and NDI inspection grid (12″ spacing between gridlines)	32
36	Deformed wing at 40% limit load	33
37	Deformed wing at 70% limit load	33
38	Deformed wing at 100% limit load	34
39	Limit load percent vs. upper wing skin strain comparison (certification vs. post-teardown full-scale tests)	35
40	Limit load percent vs. lower wing skin strain comparison (certification vs. post-teardown full-scale tests)	35
41	Spectrum loading sequence	36

LIST OF TABLES

Table		Page
1	DMA data summary for NC-8 aft wing LS samples	10
2	DMA data summary for NC-8 aft wing US samples	14
3	DSC data summary for NC-8 aft wing LS samples	18
4	DSC data summary for NC-8 aft wing US samples	20

LIST OF ABBREVIATIONS AND ACRONYMS

ASTEC	Aircraft Structural Testing and Evaluation Center
BL	Buttock line
DMA	Dynamic mechanical analysis
DSC	Differential scanning calorimetry
FS	Fuselage station
LASP	Laminate Analysis Software Package
LBL	Left buttline
LF	Lower facesheet
LS	Lower skin
LSTA	Load station location
MLG	Main landing gear
NDI	Nondestructive inspection
NIAR	National Institute for Aviation Research
OEM	Original equipment manufacturer
RBL	Right buttline
SPAID	Sandwich Panel Analysis Impact/Delamination
T_g	Glass transition temperature
TT	Tap testing
TTU	Through-transmission ultrasonic
UF	Upper facesheet
US	Upper skin
UT	Ultrasonic testing

EXECUTIVE SUMMARY

Current economic conditions require the use of military and commercial aircraft beyond their original design service objectives. Therefore, it is necessary to understand aging aircraft in-service-induced deterioration to ensure the airworthiness and structural integrity of these airframes. Most previous aging aircraft studies have focused on metallic structures. However, as more composite components are being certified and used on aircraft structural components, it is crucial to address this aging concern for composite components.

This report summarizes the findings of a study conducted on a composite carbon/epoxy Beechcraft Starship aft wing to determine the effects of aging after 12 years of service and 1800 flight hours. The Beechcraft Starship was the world's first pressurized all-composite business turboprop and received Federal Aviation Administration certification in 1987. Only 53 Starships were manufactured; production was discontinued because of low demand. Because of economic reasons and prohibitive fleet support costs, the original equipment manufacturer gathered and destroyed most of its Starship fleet. This report provides highlights of the results of the teardown study conducted on a Starship NC-8 aft wing. Results indicated that the composite structure maintained its structural integrity over its service life and did not show significant degradation or detrimental signs of aging. However, the number of flight hours was too small to interrogate the effects of mechanical fatigue.

1. INTRODUCTION

The Beechcraft Starship aft wing is the oldest primary structure in a small business aircraft built using composite materials. In the late 1970s, Beechcraft was leading the small business aircraft market following the success of its King Air twin aircraft. However, the King Air aircraft design was more than 15 years old, and company executives had concerns about losing market shares in the future if new innovative designs were not introduced. As a result, Beechcraft started work in 1979 on a new pressurized, all-composite twin-engine business turboprop—the Starship—which was the most ambitious development project in the general aviation industry at the time [1]. The objectives of the program were to design and build the most advanced turboprop aircraft by using composite materials in airframe structures. The Starship received Federal Aviation Administration certification in June 1987, and the original equipment manufacturer (OEM) built a total of 53 airframes. However, because of low demand, only a fraction of them were sold.

To characterize the structural integrity of the composite wing after it was retired from service, the National Institute for Aviation Research (NIAR) acquired the aged wing and conducted several destructive and nondestructive tests to assess its structural integrity. Generated data were used to understand aging mechanisms on composite parts currently in service and to reveal differences between damage mechanisms and damage accumulation in metallic versus composite components. These data will aid in future inspection and maintenance plans for composite structures to ensure their continued airworthiness and safety. The ultimate goal of the investigation was to assess the overall structural integrity of the composite wing after 12 years of service, to identify possible changes in the material properties due to environmental effects/flight service, to provide data to help understand aging mechanisms in composite structures, and to gain confidence in the long-term durability of composite materials.

2. BEECHCRAFT STARSHIP AFT WING TEARDOWN STUDY

The teardown of the Starship carbon fiber reinforced plastic main wing was used to evaluate the aging effects on the structural integrity of the composite structure after 12 years of service and 1800 flight hours. The research was divided into two subtasks: nondestructive and destructive. Nondestructive inspection (NDI) investigated the existence and extent of flaws introduced during manufacture or service using OEM NDI specifications. Destructive inspection/evaluation consisted of thermal analysis, physical tests, and image analysis. The generated data were compared, when possible, to the data that were generated during the aircraft design phase. A full-scale test was also conducted on the aft wing, which was subjected to the most critical static load case that the article sustained during certification. The static limit load test was followed by fatigue spectrum loading, in which the article was subjected to the equivalent of one lifetime of fatigue cycles, and was concluded with another limit load test. The objective of the test was to evaluate the structural response of the aged wing as compared to that of the article used for certification.

2.1 TEST ARTICLE DESCRIPTION

The Beechcraft Starship used for the teardown evaluation was a pressurized twin-engine turboprop with approximately 70% of composite by weight (see figure 1). The Starship was the world's first pressurized all-composite business turboprop. The aircraft has a variable sweep forward wing or

canard, rear mounted Pratt and Whitney pusher type turboprops, and twin vertical stabilizers mounted on the tips of the aft main wing. Figure 2 is a 3-view drawing of the aircraft [2].

Figure 1. Beechcraft Starship under investigation (NC-8)

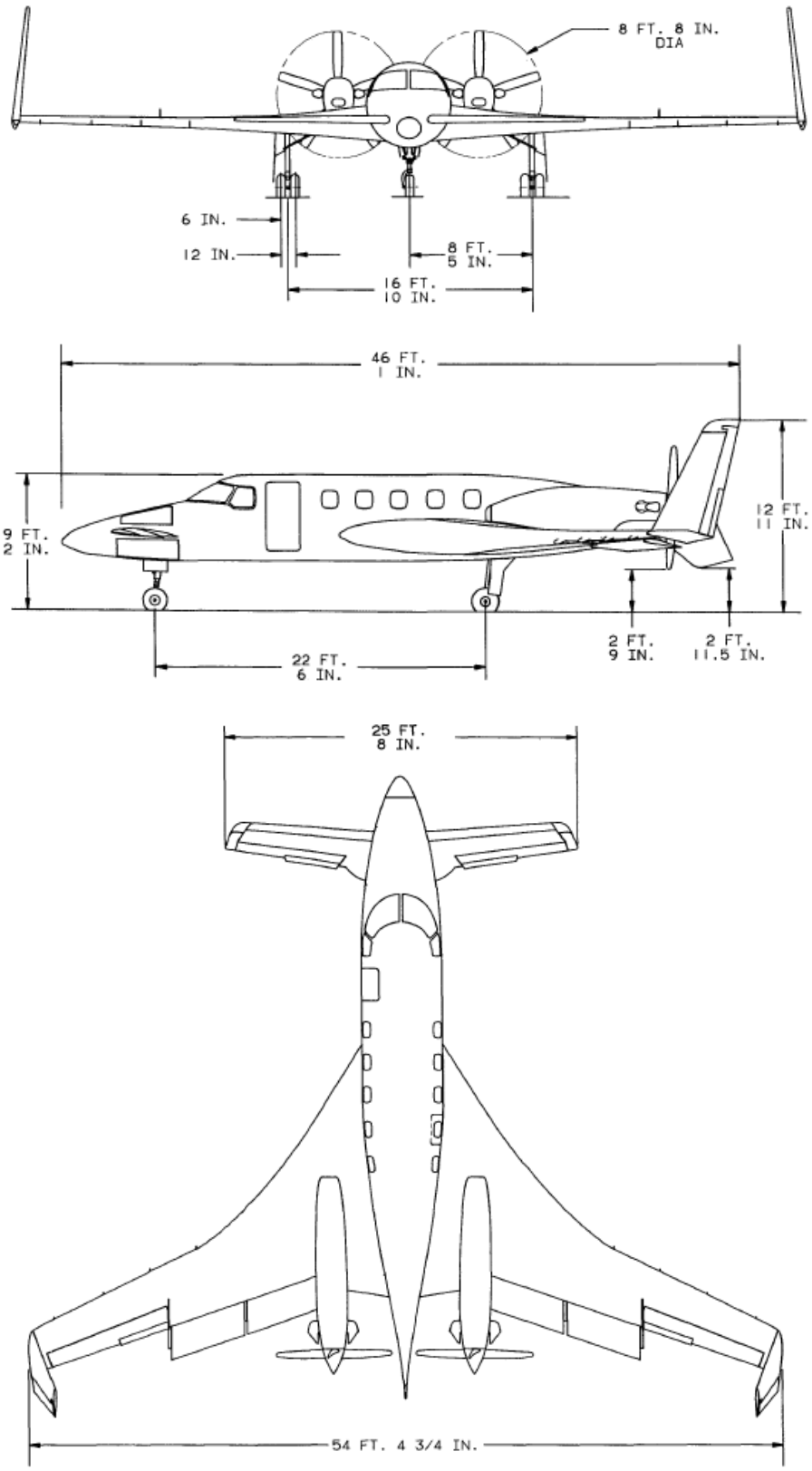

Figure 2. Beechcraft Starship airplane 3-view drawing with dimensions [2]

The structure under investigation was the NC-8 main/aft wing, which is a monocoque sandwich construction. The wing's primary structural components (skins, spars, and ribs) are sandwich panels manufactured using carbon-epoxy facesheets co-cured to a Nomex Honeycomb core [3 and 4]. The wing skins, which were cured in one piece (54′ tip-to-tip), were designed to carry bending loads similar to spar caps in a conventional wing design. During assembly, the pre-cured panels were co-bonded (secondarily bonded) together using paste adhesive. The wing assembly is shown in figure 3. In addition to the skins, the aft wing assembly incorporated three full-span spars, a main landing gear (MLG) spar, a curved leading edge spar, five full chord ribs, and an MLG rib. Skin facesheet lay-up, core density, and core thickness varied depending on the strength and stiffness requirements dictated by the loading requirements.

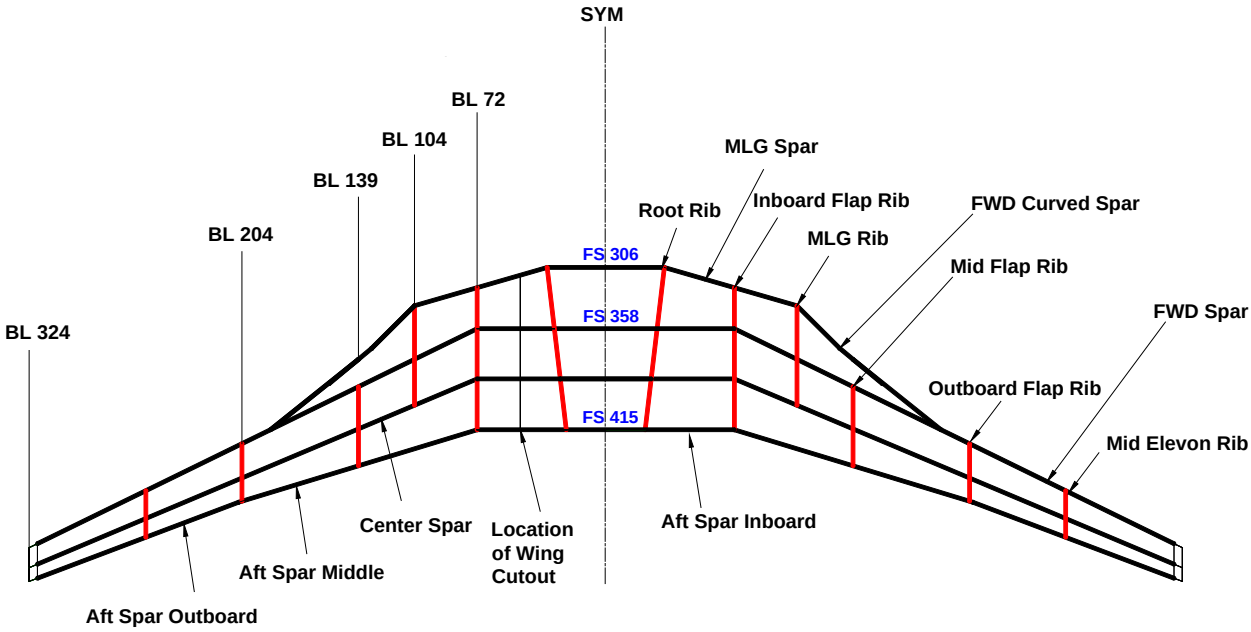

Figure 3. Beechcraft Starship aft wing structural details

The aft wing main components (skins, ribs, and spars) were cured separately and then bonded together in a secondary operation using H- and V-joints, shown in figures 4 and 5. The H-joint, a pre-cured woven graphite epoxy H-section, was bonded to the skin using film and paste adhesive, and then the spars were co-bonded to the skins using paste adhesive. Similar to the H-joint, the V-joint is a pre-cured V-section co-bonded to the skin first and then bonded to the spars using film adhesive.

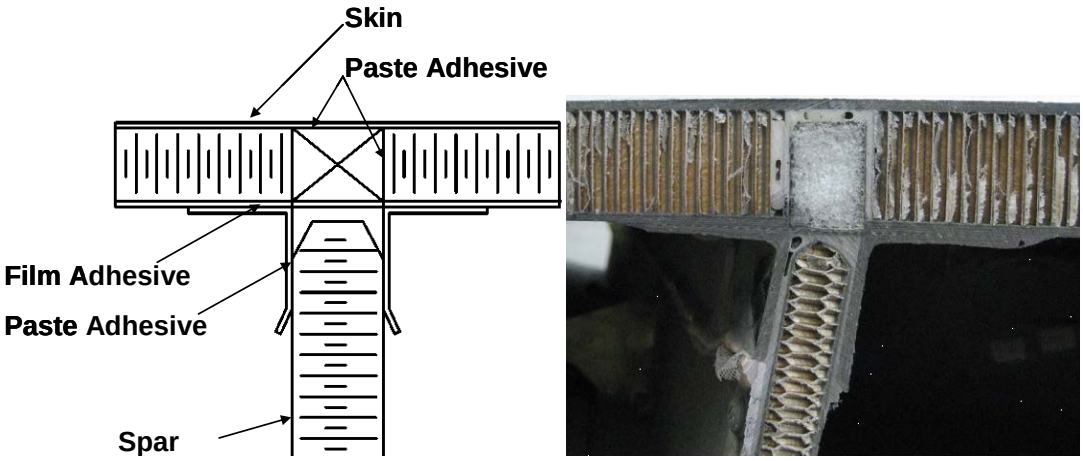

Figure 4. The (a) Starship aft wing structural H-joint details and (b) H-joint extracted from BL78 upper skin center spar

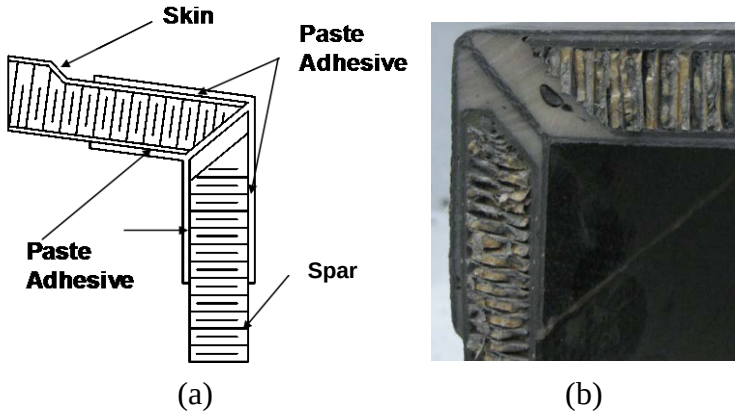

Figure 5. The (a) Starship aft wing structural V-joint details and (b) V-joint extracted from BL78 lower skin front spar

2.2 MATERIAL SELECTION

Commercially available materials at the time of the aircraft's construction were selected based on ultimate strain capability for damage tolerance requirements, resin cure temperature, and glass transition temperature (T_g) for toughness, environmental, and process requirements [4]. The material selected was AS4/E7K8, and a wide variety of material forms were used for maximum design flexibility [4]. Material qualification was conducted using the test matrices and statistical analysis methods published in the Composite Materials Handbook-17. Material qualification data established lamina properties for the various material forms.

2.3 LIGHTNING PROTECTION SCHEME

Lightning protection was achieved by using a hybrid woven graphite/aluminum fabric as the surface ply on all exterior surfaces [4]. The aluminum wires used were 0.004″ in diameter and

capable of spreading the attachment energy over a larger surface, therefore limiting damage from a 200 kA strike to the outer ply [5].

2.4 SUPPORTING DATA FOR CERTIFICATION

The Starship was certified to Title 14 Code of Federal Regulations Part 23 regulations, commuter category option, amendment 34 plus special conditions [5 and 6]. These special conditions addressed the tests and analyses needed for composite structure substantiation and included damage tolerance substantiation, residual strength substantiation, and environmental effects considerations. Certification was achieved through analysis supported by tests. Finite element analysis using MSC Nastran was conducted to determine the structure's internal loading, which was used along with analytical and test data to calculate margins of safety. Full-scale structural tests were used to validate the analytical predictions. Two analytical tools were developed and used for substantiation—Laminate Software Analysis Package (LASP) and Sandwich Panel Analysis Impact/Delamination (SPAID) [7]—and were used in conjunction with MSC Nastran.

LASP was used to calculate laminate material properties using lamina properties for various environments; it was also used to apply the internal loads from MSC Nastran to the given laminate and to compute individual ply stresses or strains. Margins of safety were then calculated using stress interaction failure criteria. The finite element model was also used for analytical predictions in a hot/wet environment using LASP hot/wet lamina properties and was validated using moisture-conditioned full-scale components. The SPAID analytical tool was used for stability analysis of panels under shear and compression loading and to predict buckling and threshold of detectability failure loads from which margins of safety could be derived.

2.5 LEFT WING-SECTION NDI

Through-transmission ultrasonic (TTU) scans of the left upper- and lower-wing skins are shown in figure 6. TTU NDI showed no major flaws in the skins induced during manufacture or service. OEM records suggest that porosity levels in the upper skin (US) flanges exceed 2.5%.

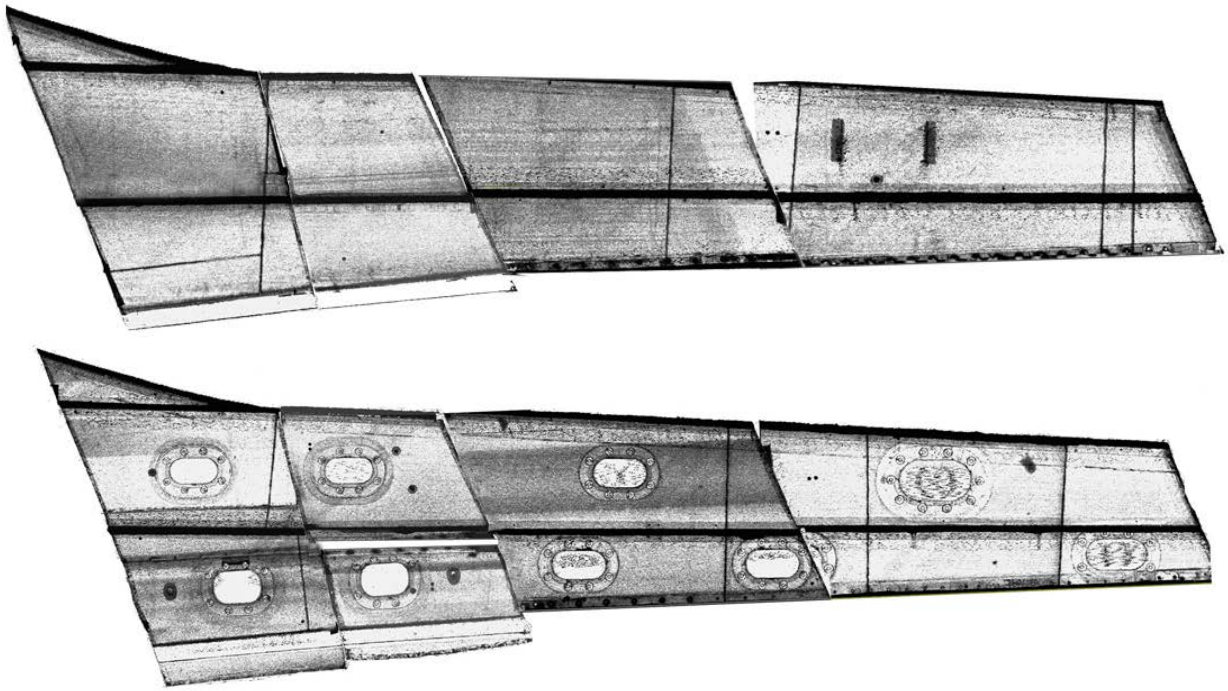

Figure 6. Beechcraft Starship aft wing TTU scans of the left upper- and lower-wing skins

2.6 THERMAL ANALYSIS

Thermal analysis was conducted on coupons extracted from both the upper and lower aft wing skins to identify possible changes in the thermal properties of the material that might have occurred during service. Coupons were extracted from the left aft wing section, as shown in figure 7. The location of the wing cutout is also shown. Because of transportation constraints, the main wing was cut into two pieces at approximately left buttline (LBL) 50. The left wing was used for destructive evaluation and the right wing was used for the full-scale test. An 8-character string was used for coupon identification. US BL75 LFX FS346, shown in figure 7, was extracted from the US sandwich structure at buttock line (BL) 75 and fuselage station (FS) 346 from the sandwich lower facesheet (LF). X is the coupon number.

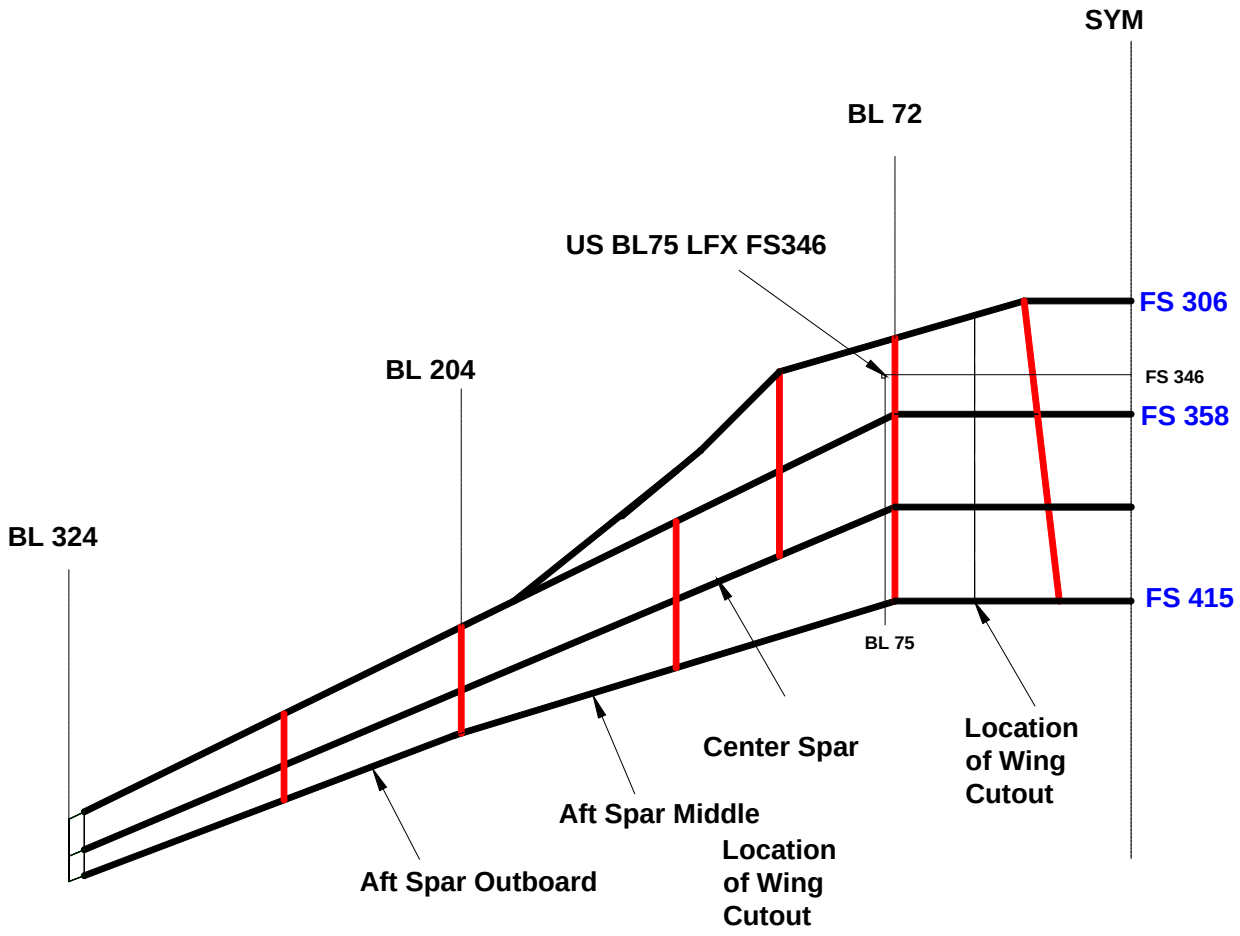

Figure 7. Aft wing coupon nomenclature

Thermal analysis tests conducted included dynamic mechanical analysis (DMA) per ASTM D7028-07 and differential scanning calorimetry (DSC) per ASTM D3418-08. DMA tests were used to interrogate the material's T_g, measure the response of a material to periodic stress, and provide information about the modulus and the damping of the material. DSC tests were used to assess the degree of cure of the material. DMA curves provide two values of T_g: a value based on the onset storage modulus or material fiber stiffness loss and a value based on material damping/maximum viscosity, which is the peak of tangent delta (tan δ), as shown in figure 8. Storage modulus is a characteristic of the material fiber stiffness, whereas damping is a characteristic of the material matrix. The T_g value, based on the onset of storage modulus, is always more conservative than the value obtained using the peak of tan δ. Figures 8 and 9 are representative DMA curves obtained for samples extracted from the lower skin (LS) upper facesheets (UF).

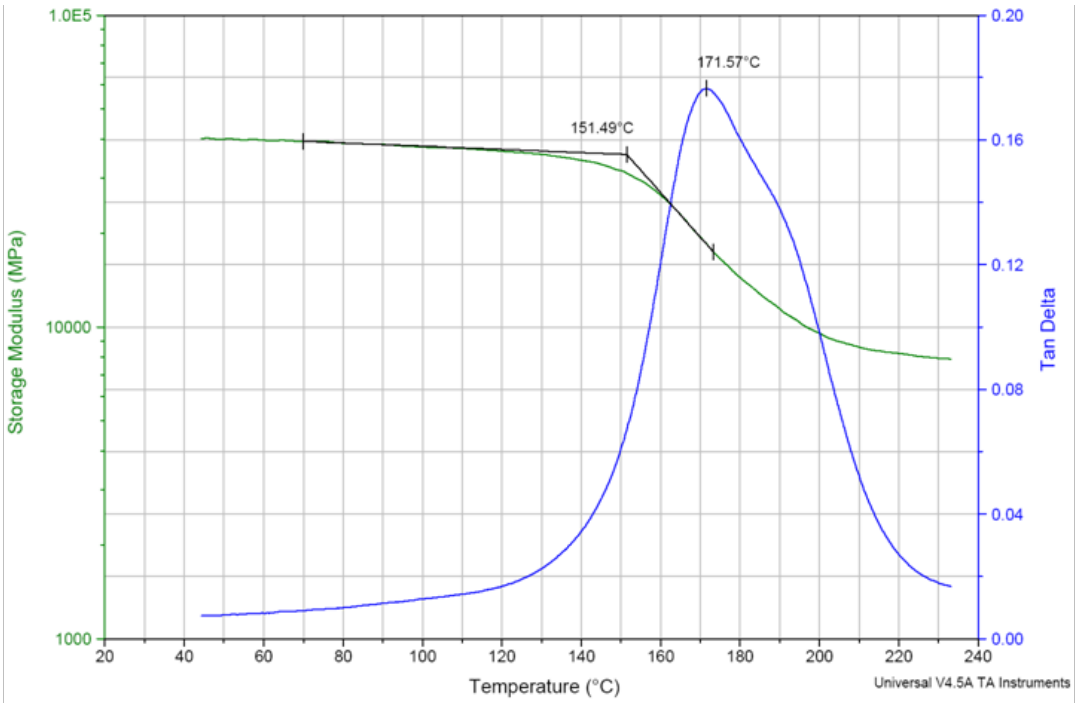

Figure 8. DMA results for sample extracted from LS BL208 UF16 FS450

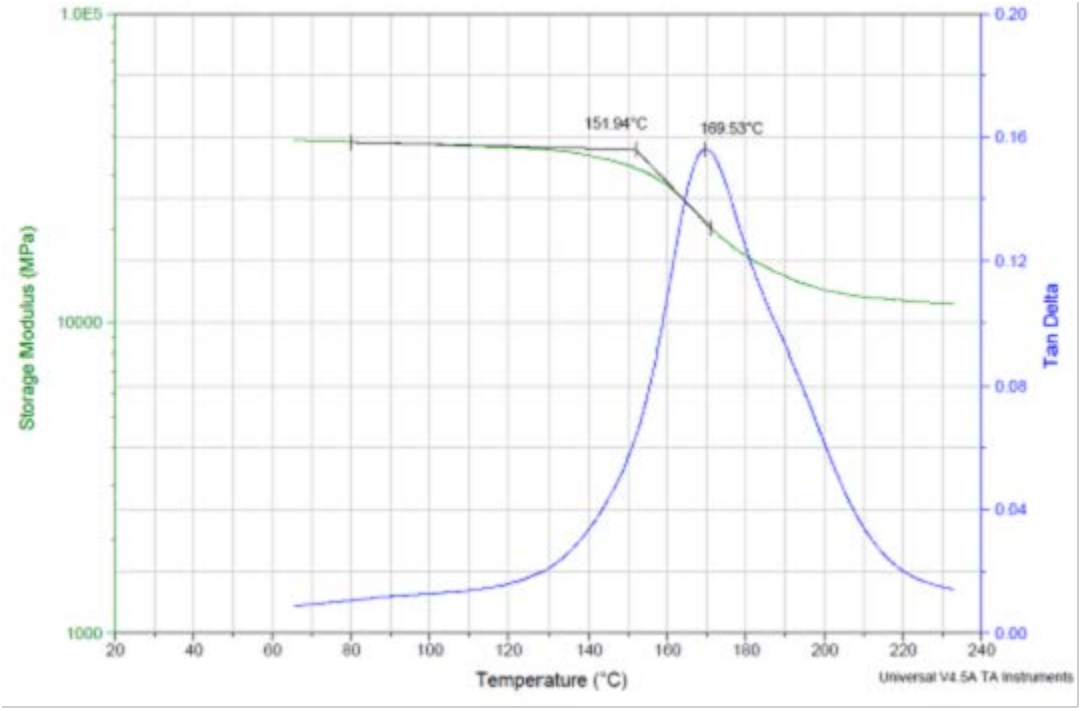

Figure 9. DMA results for sample extracted from LS BL48 UF35 FS402

A summary of the aft wing LS DMA data is shown in table 1 and figure 10. Coupons extracted from the wing LS yielded average T_g values of 153°C (307°F) (Onset of Storage Modulus) and 175°C (348°F) (Peak of tan δ).

Table 1. DMA data summary for NC-8 aft wing LS samples

DMA Test Data For LS (As Extracted)				
	Onset Storage Modulus		Peak of tan δ	
Specimen ID	T_g [°C]	T_g [°F]	T_g [°C]	T_g [°F]
LS BL48 LF35 FS402	161	322	196	385
LS BL48 LF36 FS403	162	323	194	381
LS BL48 UF35 FS402	152	305	170	337
LS BL48 UF36 FS403	149	300	175	347
LS BL50 LF25 FS391	151	303	167	333
LS BL50 LF26 FS392	151	305	166	331
LS BL50 UF25 FS391	151	304	168	334
LS BL50 UF26 FS392	150	302	167	333
LS BL74 LF15 FS369	154	308	191	375
LS BL74 LF16 FS370	156	313	172	341
LS BL74 LF25 FS402	153	307	172	342
LS BL74 LF26 FS403	151	305	170	337
LS BL74 UF15 FS369	153	307	173	343
LS BL74 UF16 FS370	152	305	170	338
LS BL74 UF25 FS402	152	306	171	339
LS BL74 UF26 FS403	152	306	172	341
LS BL142 LF5 FS403	153	308	170	338
LS BL142 LF6 FS404	154	309	170	338
LS BL142 LF15 FS429	154	308	172	341
LS BL142 LF16 FS430	153	307	170	338
LS BL142 UF5 FS403	151	304	171	340
LS BL142 UF6 FS404	153	307	170	338
LS BL142 UF15 FS429	153	308	184	364
LS BL142 UF16 FS430	153	308	172	342
LS BL208 LF5 FS434	156	313	191	376
LS BL208 LF6 FS435	158	316	191	376
LS BL208 LF15 FS449	152	305	169	336
LS BL208 LF16 FS450	151	305	170	337
LS BL208 UF5 FS434	149	300	168	334
LS BL208 UF6 FS435	148	298	167	333
LS BL208 UF15 FS449	150	303	171	339
LS BL208 UF16 FS450	151	305	172	341
LS BL260 LF5 FS459	158	317	189	373
LS BL260 LF6 FS460	159	319	193	380
LS BL260 UF5 FS459	148	299	189	371
LS BL260 UF6 FS460	148	299	178	352
Average	153	307	175	348
Standard Deviation	3	6	9	17

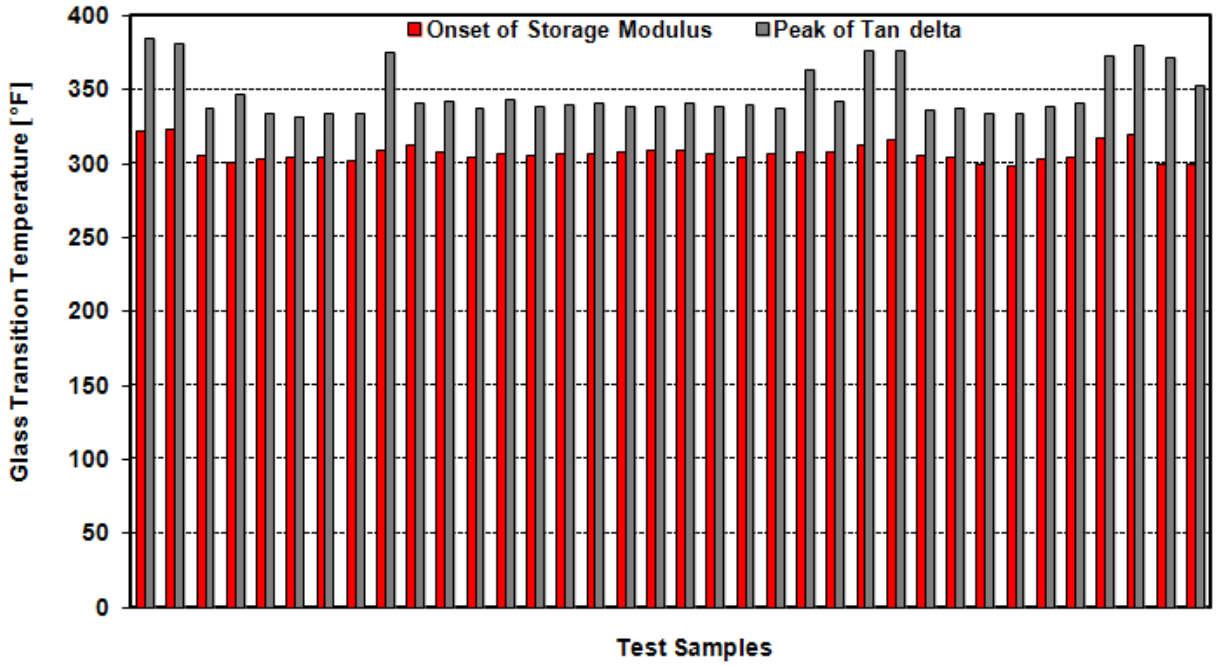

Figure 10. DMA results for coupons extracted from NC-8 aft wing LS

Figures 11, 12, and 13 are representative DMA curves obtained for samples extracted from the aft wing US facesheets. Figure 11 shows two peaks of tan δ, one occurring at 121°C (250°F) and the other at 181°C (358°F). Similarly, figure 12 also shows two peaks of tan δ, one occurring at 130°C (266°F) and the other at 180°C (356°F). DMA data shown in figures 11 and 12 are for coupons extracted from the US LF at BL 50 and BL 74. Unlike LS coupons, most of the US coupons had AF 163 film adhesive layers embedded between the plies in both facesheets. The first tan δ peak corresponds to the adhesive T_g, whereas the second peak of tan δ corresponds to the laminate resin T_g.

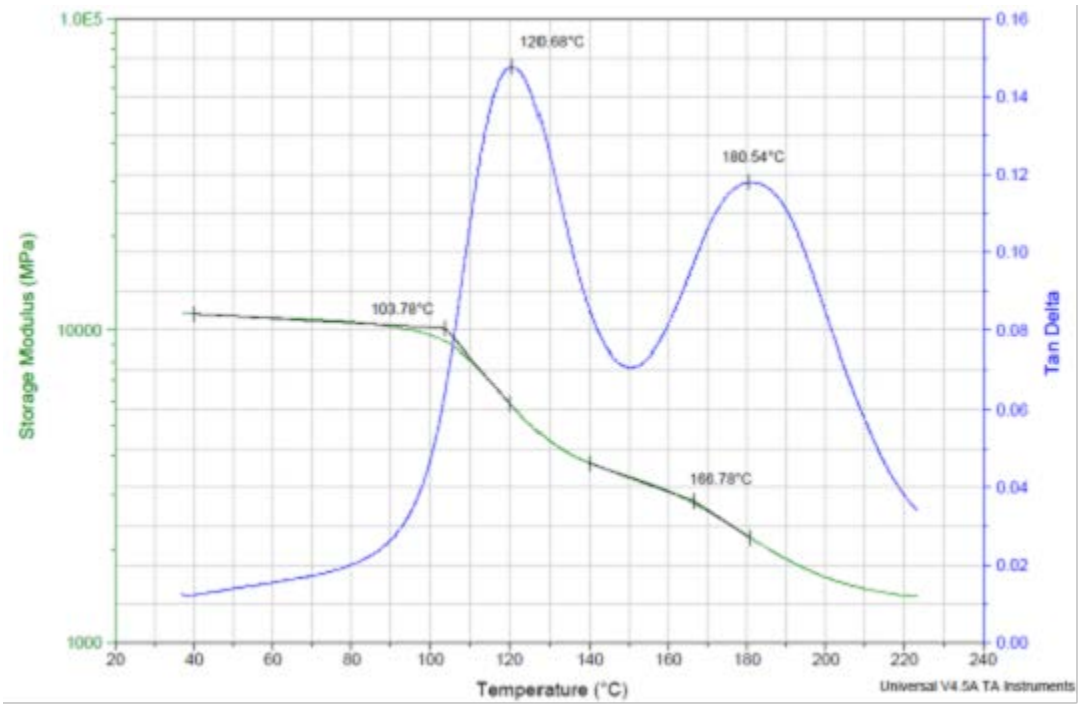

Figure 11. DMA results for a sample extracted from US BL50 LF25 FS369

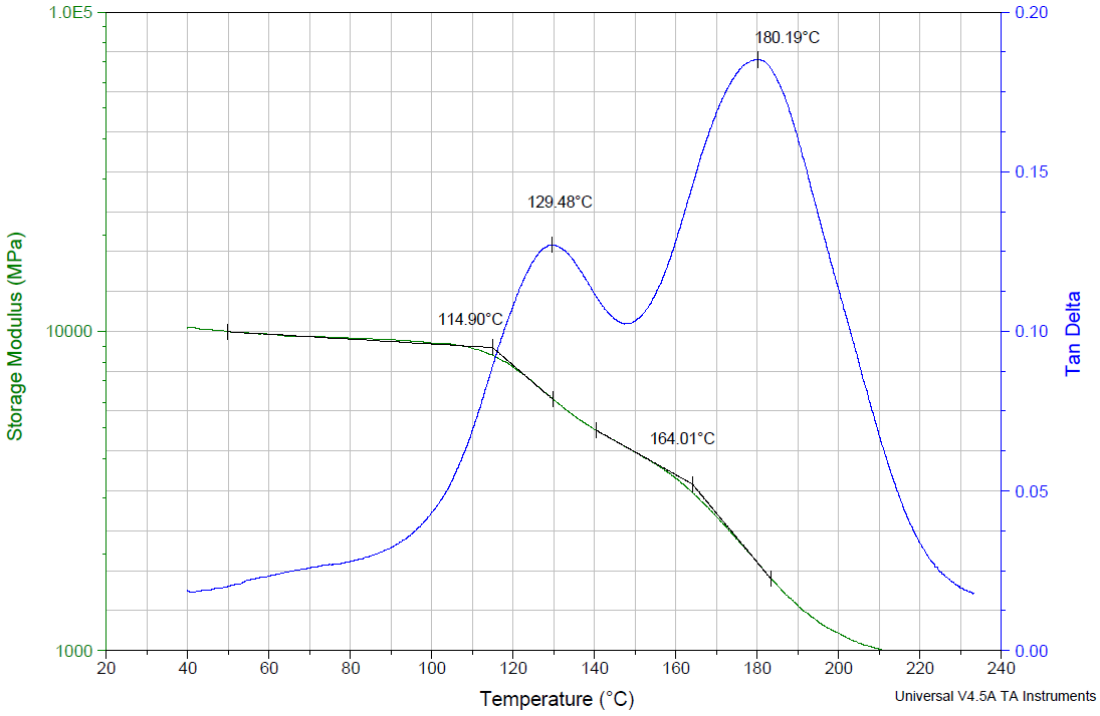

Figure 12. DMA results for a sample extracted from US BL74 LF25 FS369

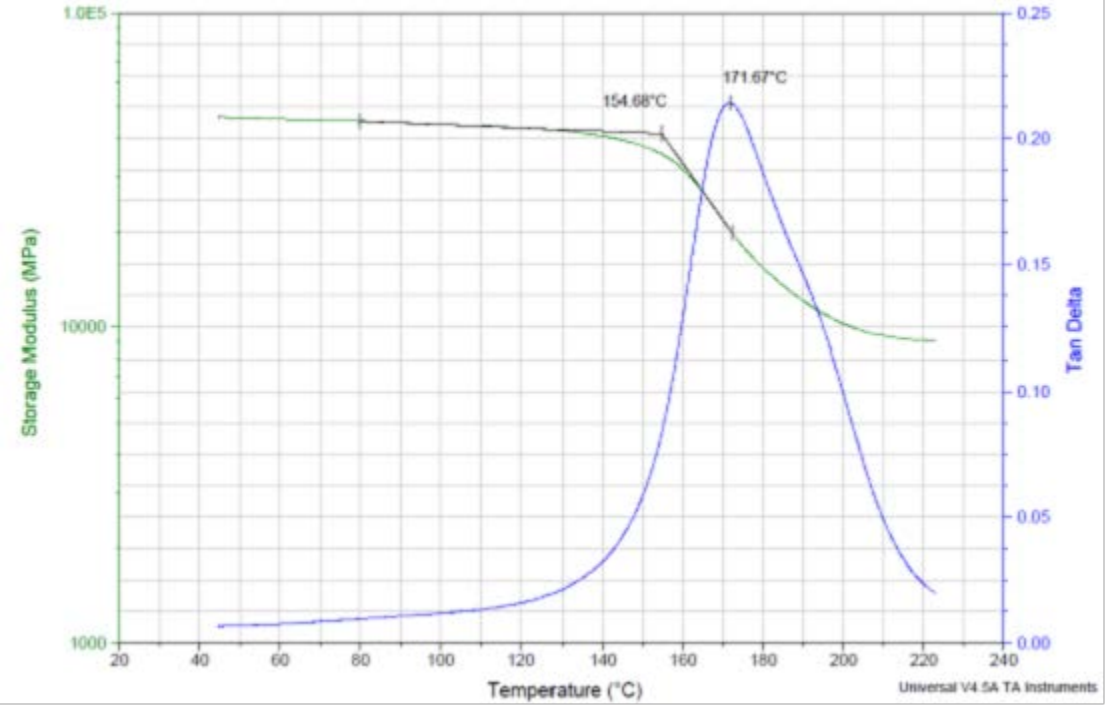

Figure 13. DMA results for a sample extracted from US BL259 UF5 FS459

A summary of the aft wing US DMA data is shown in table 2 and figure 14. Coupons extracted from the wing US yielded two T_g values for coupons extracted between LBL 48 and LBL 205. The first T_g value corresponds to that of the film adhesive that was embedded in the facesheet lay-up. The average of the first T_g was 214°F for the storage modulus and 258°F for the tan δ. The second T_g value corresponds to that of the composite laminate. The average of the second T_g was 315°F for the storage modulus and 352°F for the tan δ.

Table 2. DMA data summary for NC-8 aft wing US samples

DMA Test Data For US (As Extracted)								
Specimen ID	1st Onset Storage Modulus		1st Peak of tan δ		2nd Onset Storage Modulus		2nd Peak of tan δ	
	T_g [°C]	T_g [°F]	T_g [°C]	T_g [°F]	T_g [°C]	T_g [°F]	T_g [°C]	T_g [°F]
US BL48 LF35 FS402	101	215	128	262	169	336	185	365
US BL48 LF36 FS403	101	213	124	255	168	334	183	361
US BL48 UF35 FS402	110	230	131	267	160	320	167	332
US BL48 UF36 FS403	105	221	120	248	158	317	168	335
US BL50 LF25 FS369	104	219	121	249	167	332	181	357
US BL50 LF26 FS370	102	215	121	250	168	335	185	364
US BL50 UF25 FS369	100	212	123	253	164	328	177	351
US BL50 UF26 FS370	102	216	136	277	164	328	172	342
US BL52 LF16 FS354	96	205	116	240	157	315	175	346
US BL52 UF5 FS343	101	214	125	257	163	325	177	351
US BL52 UF15 FS353	99	210	122	251	159	318	173	344
US BL52 UF16 FS354	102	216	122	252	162	324	177	350
US BL74 LF15 FS369	105	221	134	272	161	322	173	343
US BL74 LF16 FS370	109	228	138	280	163	326	173	344
US BL74 LF26 FS403	109	228	-	-	161	321	174	345
US BL74 UF15 FS369	99	209	129	264	174	345	196	385
US BL74 UF16 FS370	99	211	120	248	160	321	192	377
US BL74 UF25 FS402	115	239	129	265	164	327	180	356
US BL74 UF26 FS403	108	227	133	271	163	325	178	353
US BL75 LF5 FS346	105	221	126	259	163	326	170	338
US BL75 UF6 FS347	98	209	-	-	157	315	173	343
US BL139 LF5 FS401	95	202	117	243	159	318	176	348
US BL139 LF6 FS402	100	211	121	251	160	320	178	353
US BL139 UF5 FS401	96	205	-	-	160	320	189	372
US BL139 UF6 FS402	97	206	-	-	161	322	190	373
US BL140 LF15 FS429	-	-	-	-	143	289	171	340
US BL140 LF16 FS430	-	-	-	-	137	279	170	338
US BL140 UF15 FS429	91	196	-	-	156	314	170	338
US BL140 UF16 FS430	86	187	114	237	154	309	167	333
US BL205 LF5 FS434	-	-	-	-	133	271	168	335
US BL205 LF6 FS435	-	-	-	-	133	271	167	333
US BL205 UF5 FS434	96	204	134	273	161	322	178	353
US BL205 UF6 FS435	103	217	129	265	172	341	194	381
US BL207 LF15 FS444	-	-	-	-	139	282	187	369
US BL207 LF16 FS445	-	-	-	-	143	290	186	366
US BL207 UF15 FS444	-	-	-	-	140	284	170	338
US BL207 UF16 FS445	-	-	-	-	148	298	179	354
US BL259 LF5 FS459	-	-	-	-	154	310	196	384
US BL259 LF6 FS460	-	-	-	-	151	304	172	342
US BL259 UF5 FS459	-	-	-	-	155	310	172	341
US BL259 UF6 FS460	-	-	-	-	156	313	171	341
Average	101	214	126	258	157	315	178	352
Standard Deviation	6	11	7	12	10	18	8	15

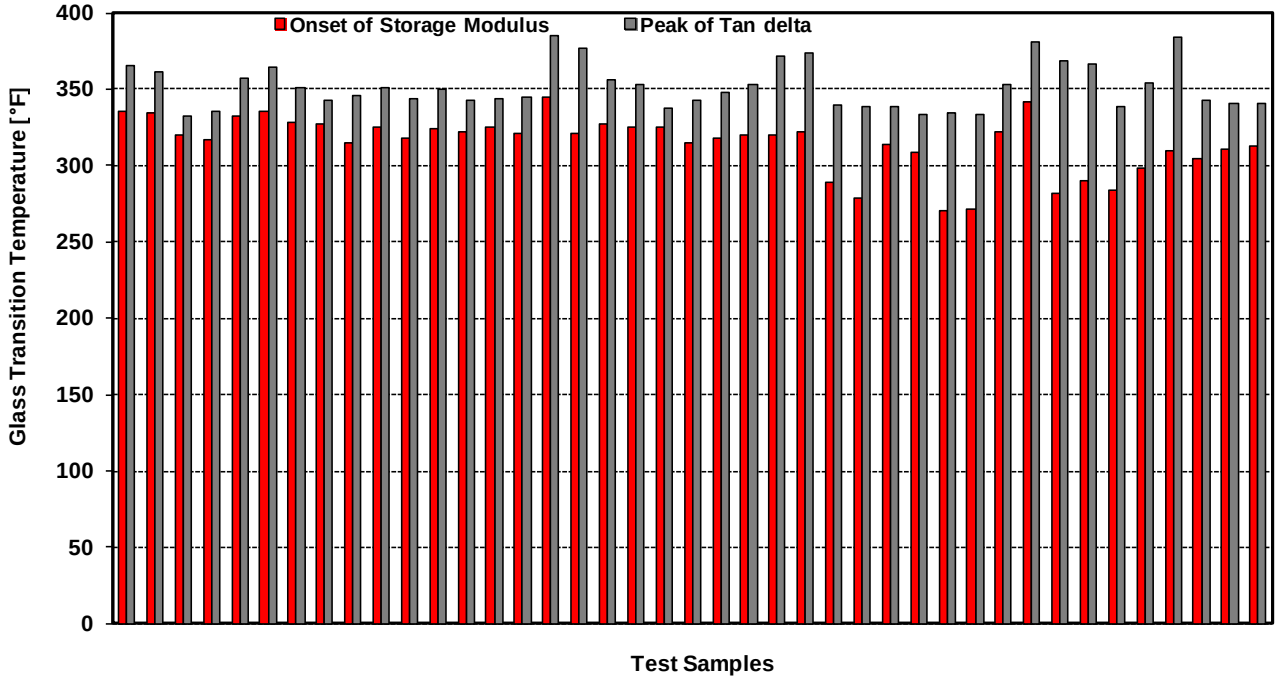

Figure 14. DMA results for coupons extracted from NC-8 aft wing US

DSC tests, per ASTM D3418-03, were conducted on specimens extracted from both skins to evaluate the degree of cure of the material. In a DSC test, samples are heated at a constant rate, and the difference in heat input between the test sample and a reference material due to energy changes is monitored. Transitions due to changes in morphological or chemical reactions in a polymer can be detected as the sample is heated, and the corresponding changes in heat flow and specific heat capacity are calculated.

Representative DSC heat flow curves obtained for the aft wing LSs are shown in figures 15–17. To evaluate the degree of cure of the aged structure, a DSC test was conducted on a T650/E7K8 prepreg sample to determine the heat of reaction required to fully cure the sample yielding 145.7 J/g. All the heat of reaction values obtained from subsequent tests were normalized with respect to this value to obtain a cure conversion percentage indicative of the degree of cure of the part.

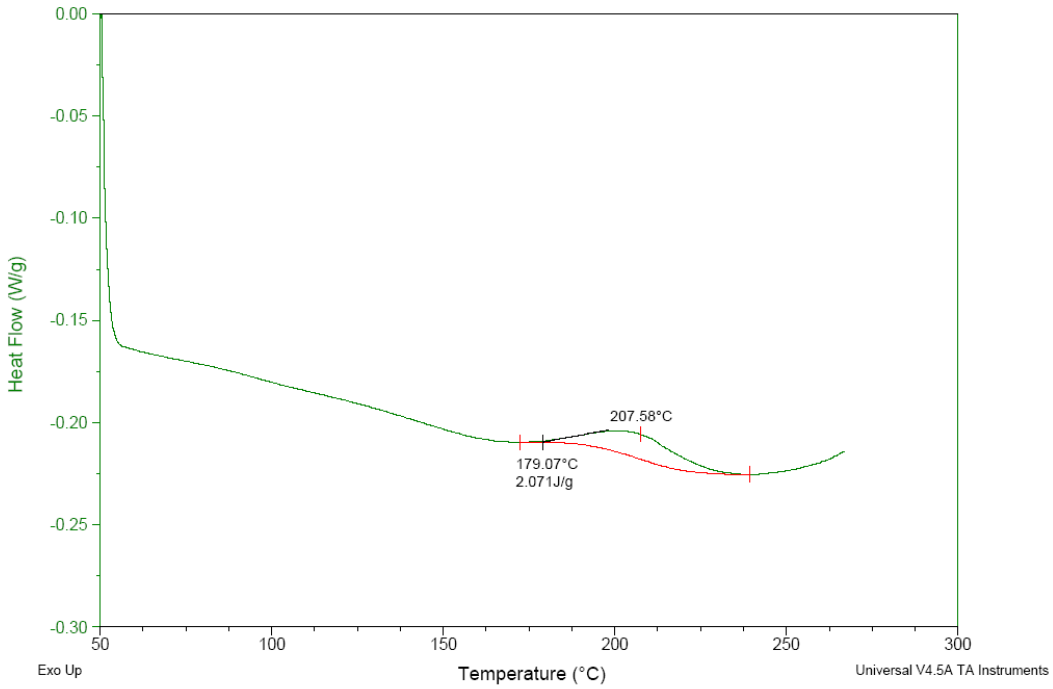

Figure 15. DSC data for a sample extracted from LS BL50 LF28 FS 394

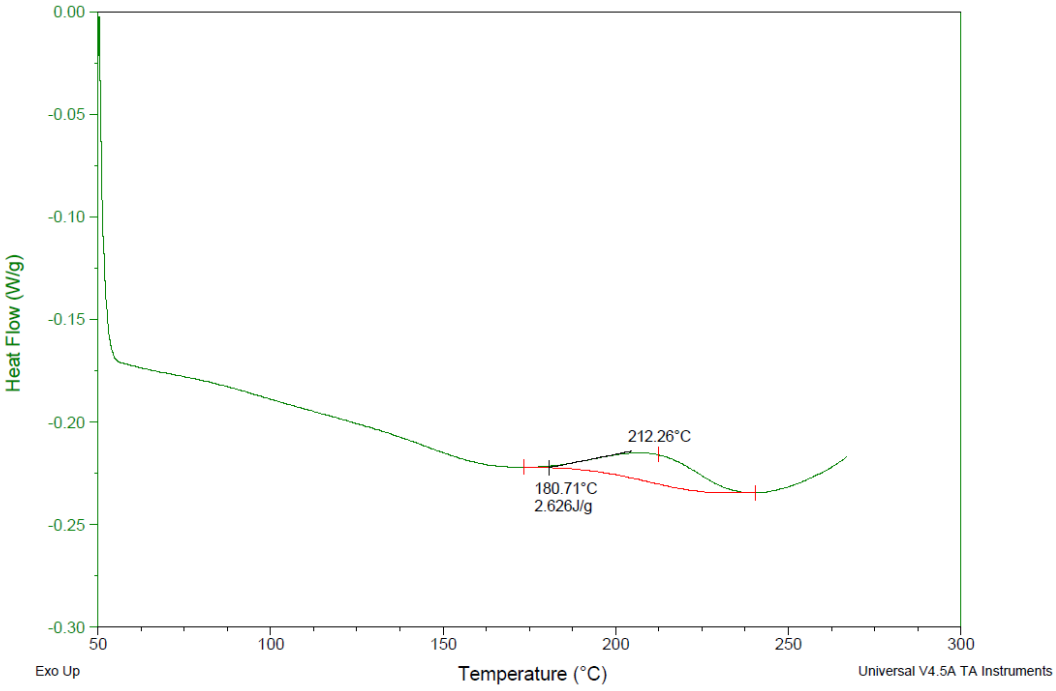

Figure 16. DSC data for a sample extracted from LS BL48 UF38 FS405

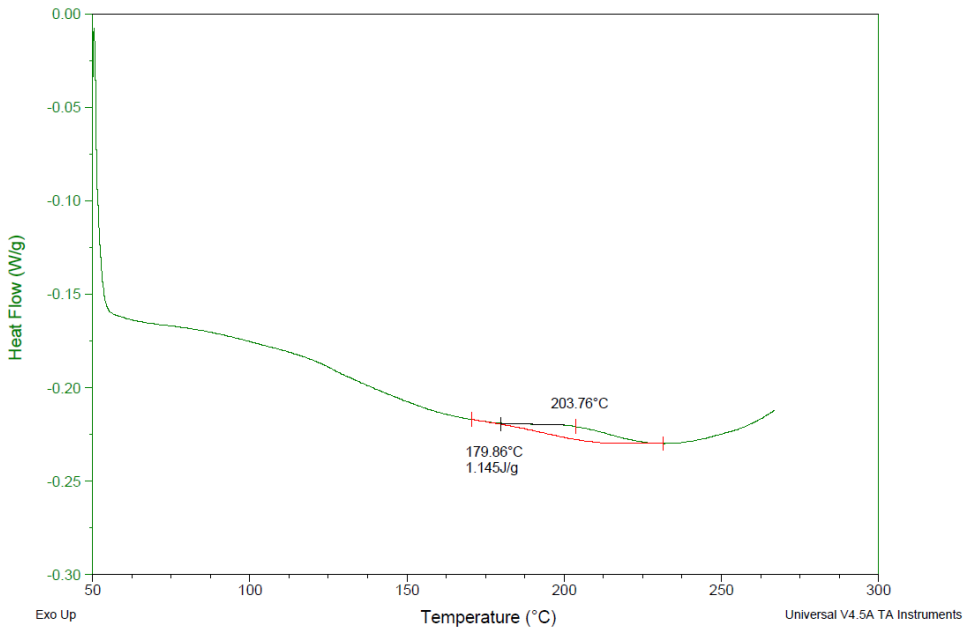

Figure 17. DSC data for a sample extracted from LS BL260 UF7 FS461

A summary of the aft wing LS DSC data is shown in table 3. Tests yielded an average heat of reaction of 2.31 J/g, an average exotherm onset temperature of 183°C (361°F), and an average exotherm peak of 211°C (413°F). This is equivalent to a 98.4% cure conversion percentage for cured LS samples.

Table 3. DSC data summary for NC-8 aft wing LS samples

DSC Results, LS						
Specimen ID	Extrapolated Onset Temperature of Exotherm		Peak Temperature of Exotherm		Heat of Reaction of Exotherm	Cure Conversion
	Ts [°C]	*Ts* [°F]	*Tp* [°C]	*Tp* [°F]	*H* [J/g]	%
LS BL48 UF37 FS404	189	371	216	421	2.14	98.5
LS BL48 UF38 FS405	181	357	212	414	2.63	98.2
LS BL50 LF27 FS393	181	358	209	408	1.62	98.9
LS BL50 LF28 FS394	179	354	208	406	2.07	98.6
LS BL50 UF27 FS393	194	382	220	429	0.61	99.6
LS BL50 UF28 FS394	180	356	213	416	2.06	98.6
LS BL74 LF17 FS371	180	356	205	402	2.05	98.6
LS BL74 LF18 FS372	179	354	209	407	2.56	98.2
LS BL74 LF27 FS404	184	364	211	413	2.08	98.6
LS BL74 LF28 FS405	182	359	210	410	2.21	98.5
LS BL74 UF17 FS371	186	366	218	424	2.69	98.2
LS BL74 UF18 FS372	181	358	213	415	3.56	97.6
LS BL74 UF27 FS404	181	357	213	416	3.54	97.6
LS BL74 UF28 FS405	181	357	214	417	3.54	97.6
LS BL142 LF7 FS405	179	354	212	414	2.93	98.0
LS BL142 LF8 FS406	180	357	209	408	2.47	98.3
LS BL142 LF17 FS431	182	359	212	413	2.46	98.3
LS BL142 LF18 FS432	182	359	214	416	3.09	97.9
LS BL142 UF7 FS405	180	357	213	415	4.01	97.2
LS BL142 UF8 FS406	186	367	215	420	2.99	97.9
LS BL142 UF17 FS431	177	350	214	417	5.96	95.9
LS BL142 UF18 FS432	186	367	213	416	2.87	98.0
LS BL208 LF7 FS436	179	354	204	399	0.73	99.5
LS BL208 LF8 FS437	180	356	207	405	0.92	99.4
LS BL208 LF17 FS451	185	364	211	412	1.05	99.3
LS BL208 LF18 FS452	182	359	214	417	3.33	97.7
LS BL208 UF7 FS436	184	363	208	406	0.54	99.6
LS BL208 UF8 FS437	193	379	213	416	0.22	99.8
LS BL208 UF17 FS451	179	355	214	416	4.02	97.2
LS BL208 UF18 FS452	179	353	211	411	2.64	98.2
LS BL260 LF7 FS461	184	363	209	409	0.85	99.4
LS BL260 UF7 FS461	180	356	204	399	1.15	99.2
LS BL260 UF8 FS462	190	373	210	410	0.55	99.6
Average	183	361	211	413	2.31	98.4
Stdev	4.1	7.4	3.7	6.6	1.3	0.9

Representative DSC heat flow curves obtained for the aft wing USs are shown in figures 18 and 19. A summary of the aft wing US DSC data is shown in table 4. Tests yielded an average heat of reaction of 1.37 J/g, an average exotherm onset temperature of 186°C (367°F), and an average exotherm peak of 212°C (414°F). This is equivalent to a 99.1% cure conversion percentage for cured US samples.

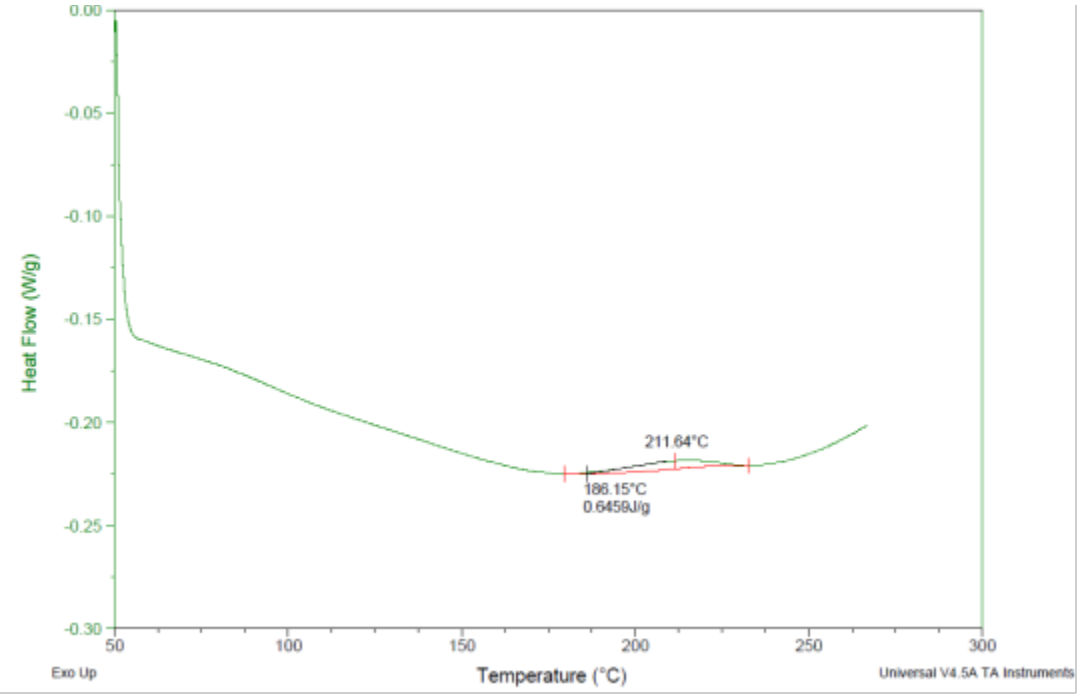

Figure 18. DSC data for a sample extracted from US BL50 LF27 FS 371

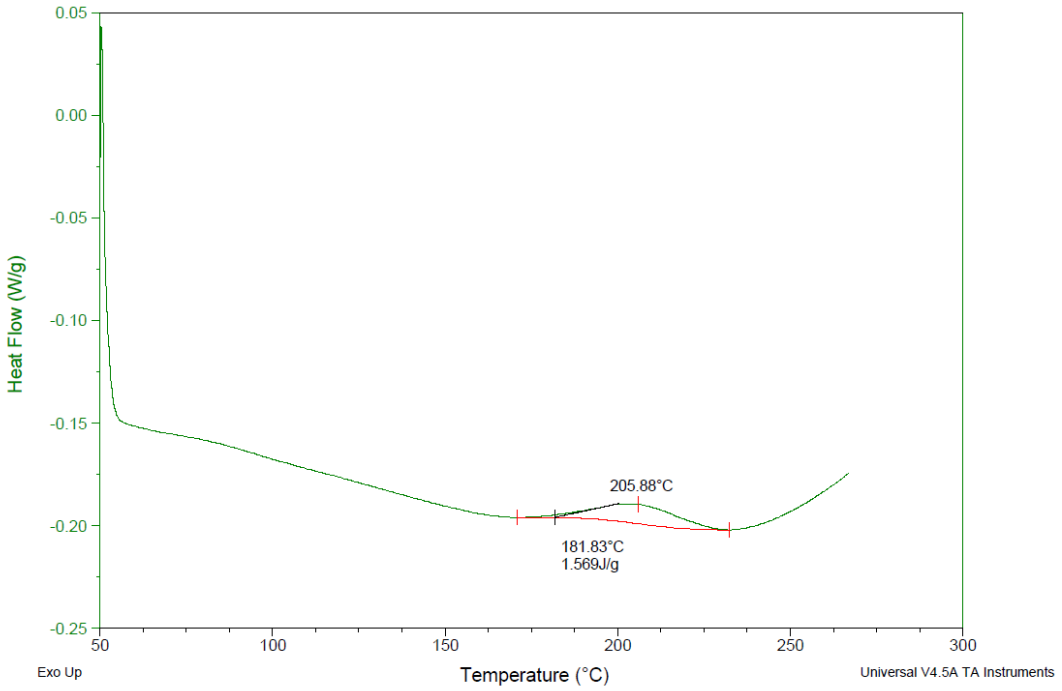

Figure 19. DSC data for a sample extracted from US BL74 LF17 FS 371

Table 4. DSC data summary for NC-8 aft wing US samples

DSC Results, US						
Specimen ID	Extrapolated Onset Temperature of Exotherm		Peak Temperature of Exotherm		Heat of Reaction of Exotherm	Cure Conversion
	Ts [°C]	*Ts* [°F]	*Tp* [°C]	*Tp* [°F]	*H* [J/g]	%
US BL48 LF37 FS404	194	382	205	400	0.28	99.8
US BL50 LF27 FS371	186	367	212	413	0.65	99.6
US BL50 UF28 FS372	187	369	209	409	0.41	99.7
US BL52 LF18 FS356	188	370	207	405	0.44	99.7
US BL52 UF7 FS345	191	375	207	404	0.21	99.9
US BL52 UF18 FS356	189	371	207	405	0.42	99.7
US BL74 LF17 FS371	182	359	206	403	1.57	98.9
US BL74 LF18 FS372	183	361	208	406	1.62	98.9
US BL74 LF28 FS405	184	364	211	413	1.18	99.2
US BL74 UF18 FS372	182	360	213	416	1.41	99.0
US BL74 UF27 FS404	193	380	216	420	0.74	99.5
US BL74 UF28 FS405	187	369	215	419	1.79	98.8
US BL75 LF7 FS348	181	357	208	407	1.47	99.0
US BL75 UF7 FS348	187	369	215	418	2.25	98.5
US BL75 UF8 FS349	189	373	214	417	1.21	99.2
US BL139 LF7 FS403	184	363	211	412	1.77	98.8
US BL139 LF8 FS404	187	369	213	415	1.04	99.3
US BL139 UF7 FS403	188	370	214	417	2.06	98.6
US BL139 UF8 FS404	190	374	216	421	1.69	98.8
US BL140 LF17 FS431	185	364	213	415	1.49	99.0
US BL140 LF18 FS432	180	357	215	418	0.82	99.4
US BL140 UF17 FS431	188	370	214	417	0.92	99.4
US BL140 UF18 FS432	189	372	207	405	1.65	98.9
US BL205 LF7 FS436	186	366	215	420	1.35	99.1
US BL205 LF8 FS437	191	377	215	419	0.95	99.3
US BL205 UF7 FS436	188	371	216	421	0.61	99.6
US BL205 UF8 FS437	195	384	216	421	0.52	99.6
US BL207 LF17 FS446	183	361	212	414	1.21	99.2
US BL207 LF18 FS447	183	362	216	421	2.99	97.9
US BL207 UF18 FS447	187	369	214	418	1.08	99.3
US BL259 LF7 FS461	181	358	212	414	2.04	98.6
US BL259 LF8 FS462	182	359	209	408	1.85	98.7
US BL259 UF7 FS461	184	362	216	420	3.17	97.8
US BL259 UF8 FS462	179	355	213	416	3.83	97.4
Average	186	367	212	414	1.37	99.1
Standard Deviation	4.1	7.3	3.5	6.2	0.8	0.6

2.7 Moisture Content Evaluation

Moisture content in the aged structure was quantified with ASTM D5229 using coupons extracted from both skins. The maximum moisture content was 1.1% for the US and 1.3% for the LS. This is consistent with the moisture analysis data generated by the OEM and the moisture analysis data published in the NASA report [8], which predicted a 1.1% ± 0.1% total weight gain expected in the structure in service due to moisture uptake. Sample moisture desorption curves as a function of time for coupons extracted from the LS are shown in figures 20 and 21. These data are also consistent with moisture absorption evaluation tests conducted by the OEM.

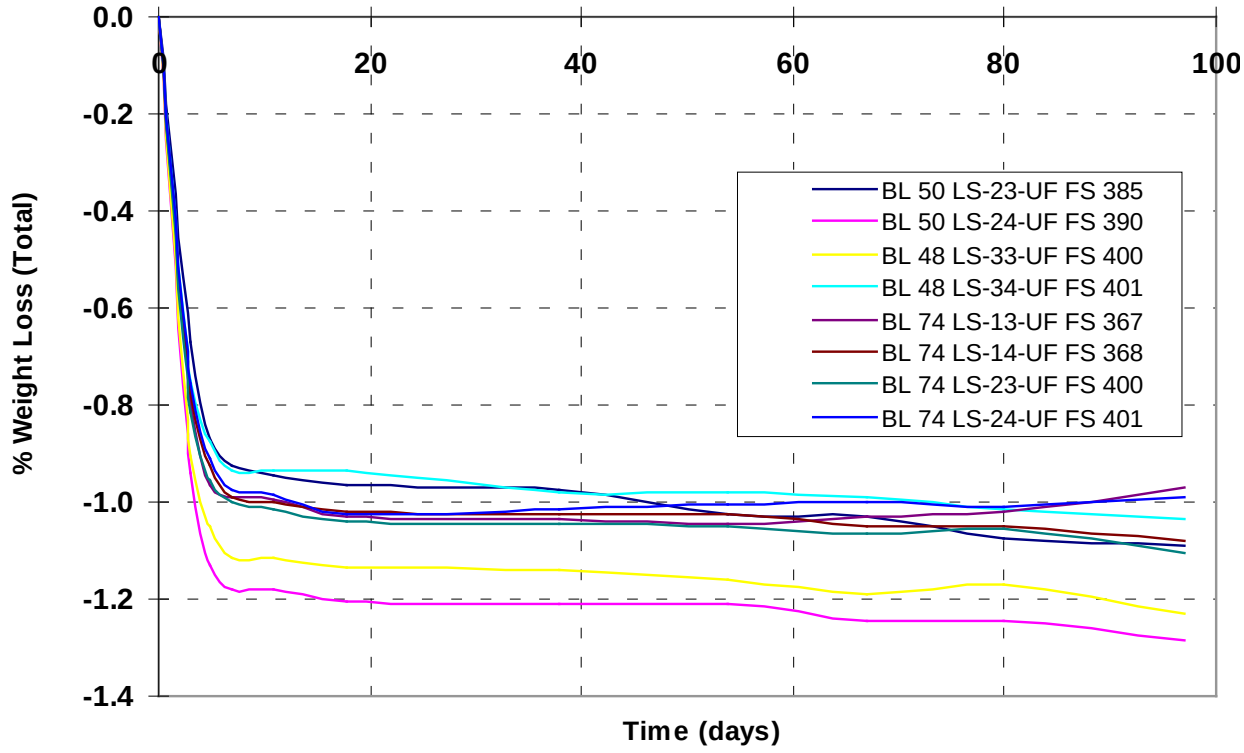

Figure 20. Moisture loss as function of time for coupons extracted from LS

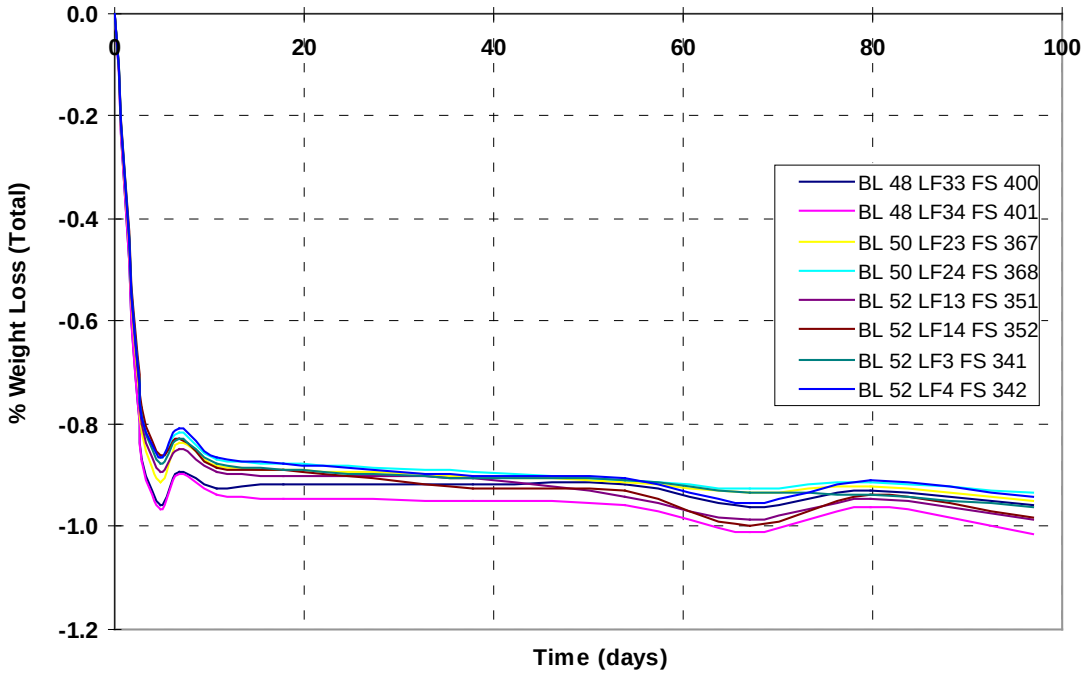

Figure 21. Moisture loss as a function of time for coupons extracted from the US

2.8 Microscopy

Image analysis was conducted on samples extracted from both the USs and LSs to inspect the structure microscopically for voids, microcracks, or any evidence of aging or material degradation. Extracted samples were potted, polished, and viewed under a microscope to detect any evidence of material aging. Various images showed scattered porosity in the adhesive layer between the plies, as shown in figures 22–29. Porosity, present in the adhesive plies of the US facesheets, was possibly caused by a combination of the resin and adhesive system (low flow) and the material form (fabric inherently entraps more air than tape).

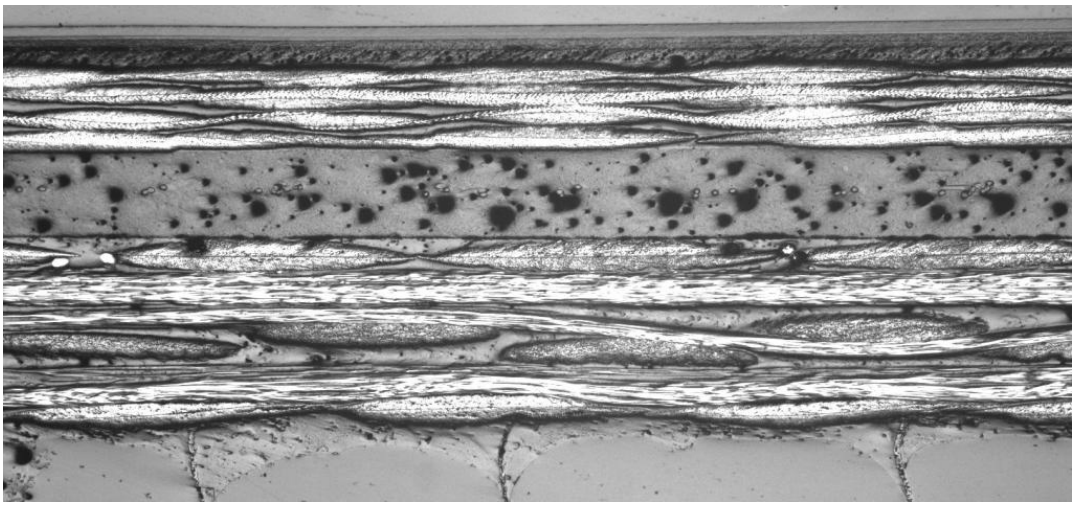

Figure 22. US BL48 UF 39

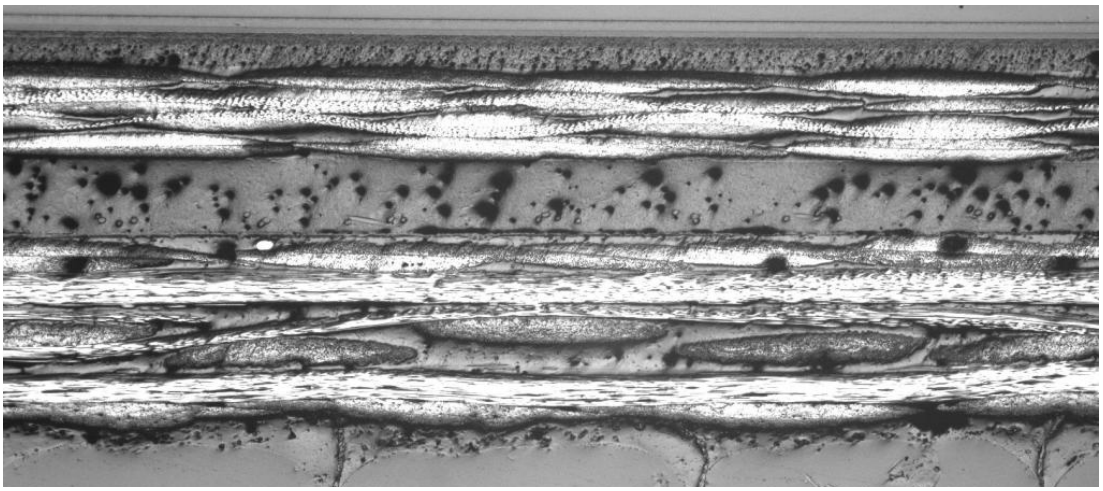

Figure 23. US BL48 UF 40

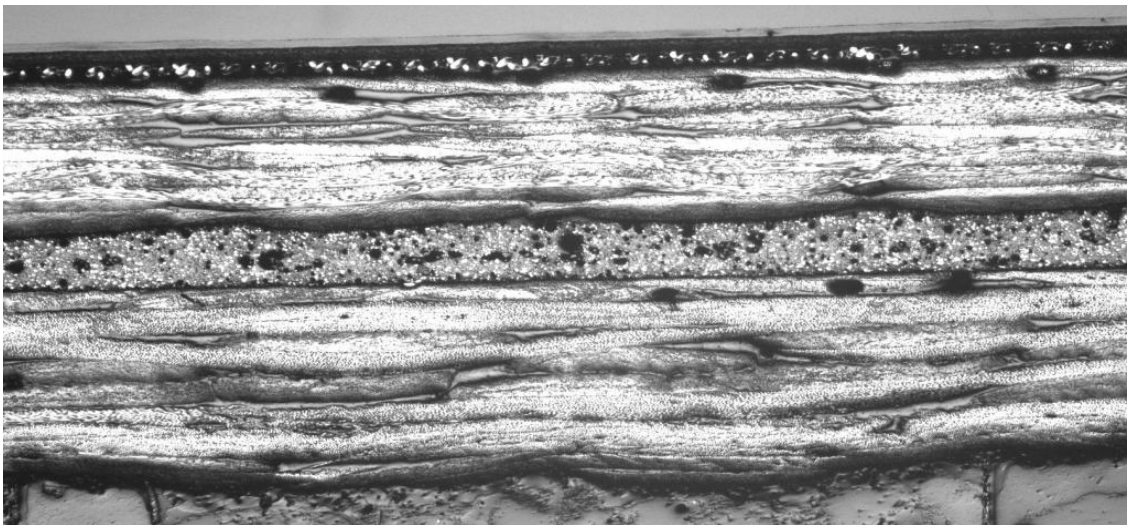

Figure 24. US BL140 UF 20

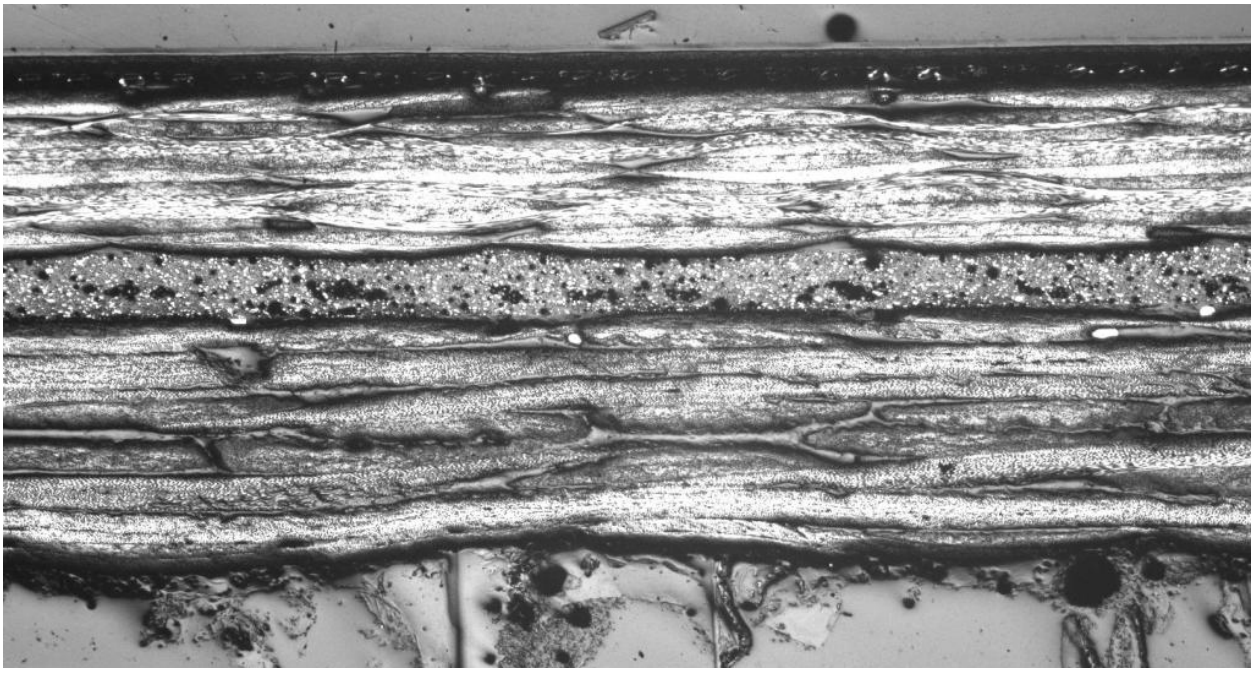

Figure 25. US BL140 UF 19

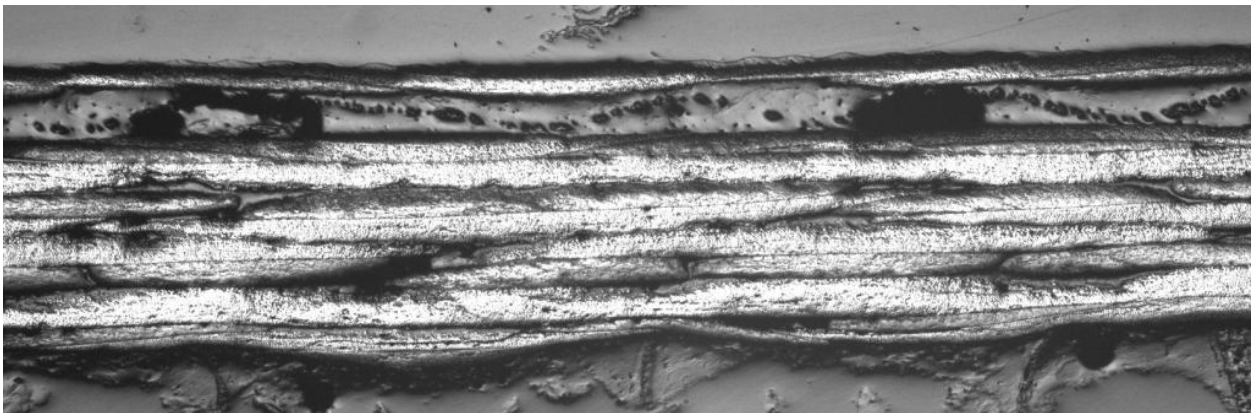

Figure 26. US BL140 LF 19

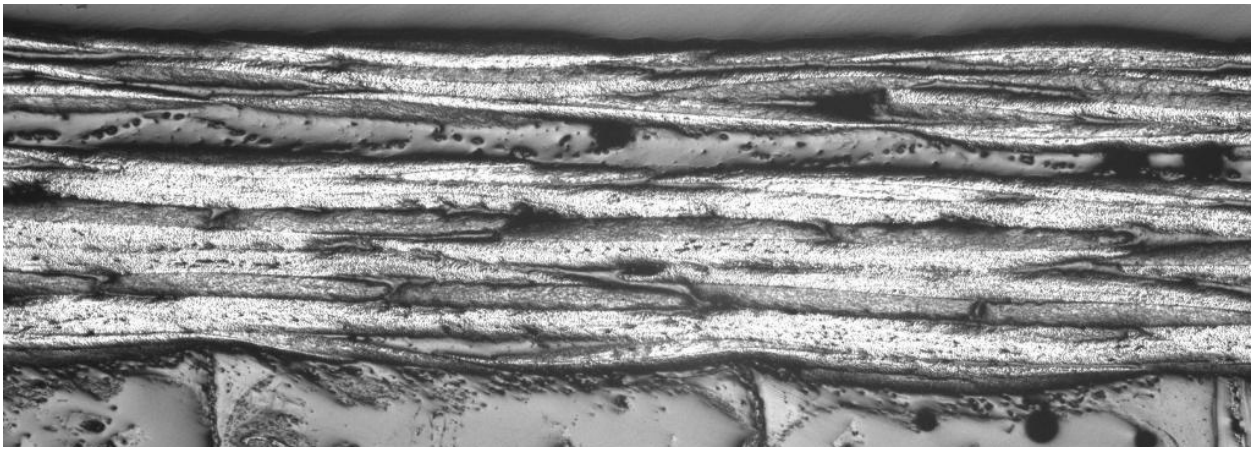

Figure 27. US BL140 LF 20

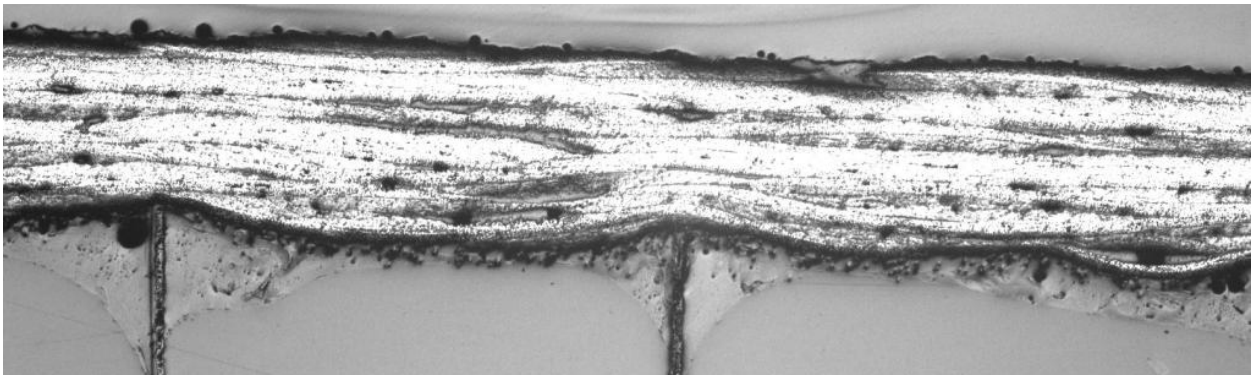

Figure 28. LS BL74 LF 29

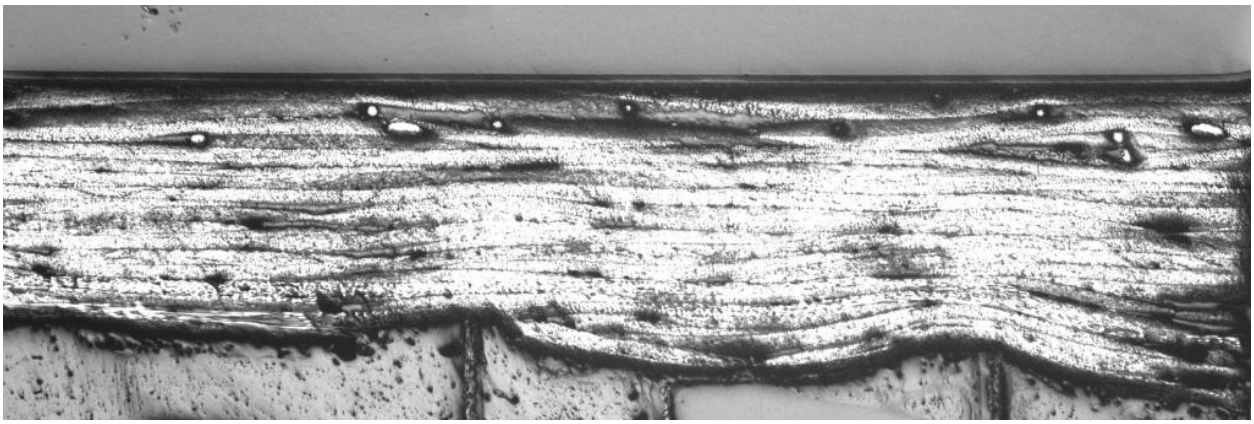

Figure 29. LS BL208 UF 20

2.9 Starship Aft Wing Full-Scale Test

2.9.1 Full-Scale Article—NDI

Because of transportation constraints, the main wing was cut into two pieces at approximately LBL 50. The left wing was used for destructive evaluation and the right was used for the full-scale test.

The initial evaluation of the left aft wing section as a baseline was conducted at the Aircraft Structural Testing and Evaluation Center (ASTEC) at NIAR. A baseline NDI was conducted according to OEM specifications prior to subjecting the structure to a limit load test. An NDI grid was drawn on the structure for ease of inspection and flaw-growth monitoring. Visual inspection, TTU scans, and tap testing (TT) were used for the inspection. The TT was conducted on the entire wing surface and a back-up inspection using ultrasonic testing (UT) was conducted if any suspicious areas were detected. Coupons were extracted from various areas in the wing LBL and were used as reference standards to inspect the wing right buttline (RBL). Once the initial inspection was completed, subsequent inspections were conducted after the first limit load test and on completion of the cyclic testing. For the initial inspection, all accessible skin, ribs, spars, and corresponding joints were thoroughly inspected for manufacturing defects, delaminations, disbonds, or any other manufacturing or in-service damage. All defects were documented and monitored for growth during the subsequent inspections.

The initial TT examination of the upper aft wing skin did not reveal any damage or defects in the test section (RBL 100-RBL324), but revealed a potential disbond in one location. This area was inspected with the back-up UT procedure for verification. The UT confirmed the disbond in an area approximately 15.50″ x 12.00″. The disbond is believed to have been caused by the removal of the engine. Once the engine was pulled from the wing, it appeared that the skin may have been ripped away from the structure, which caused the disbonding. An overview of the disbond of the right upper aft wing is shown in figure 30. The damaged area was repaired using a wet lay-up bonded repair, according to the OEM specifications. During the repair, it was found that the area identified as a disbond was potted and that the UT and TT signals obtained were caused by sound attenuation through the potting material and not because of damage.

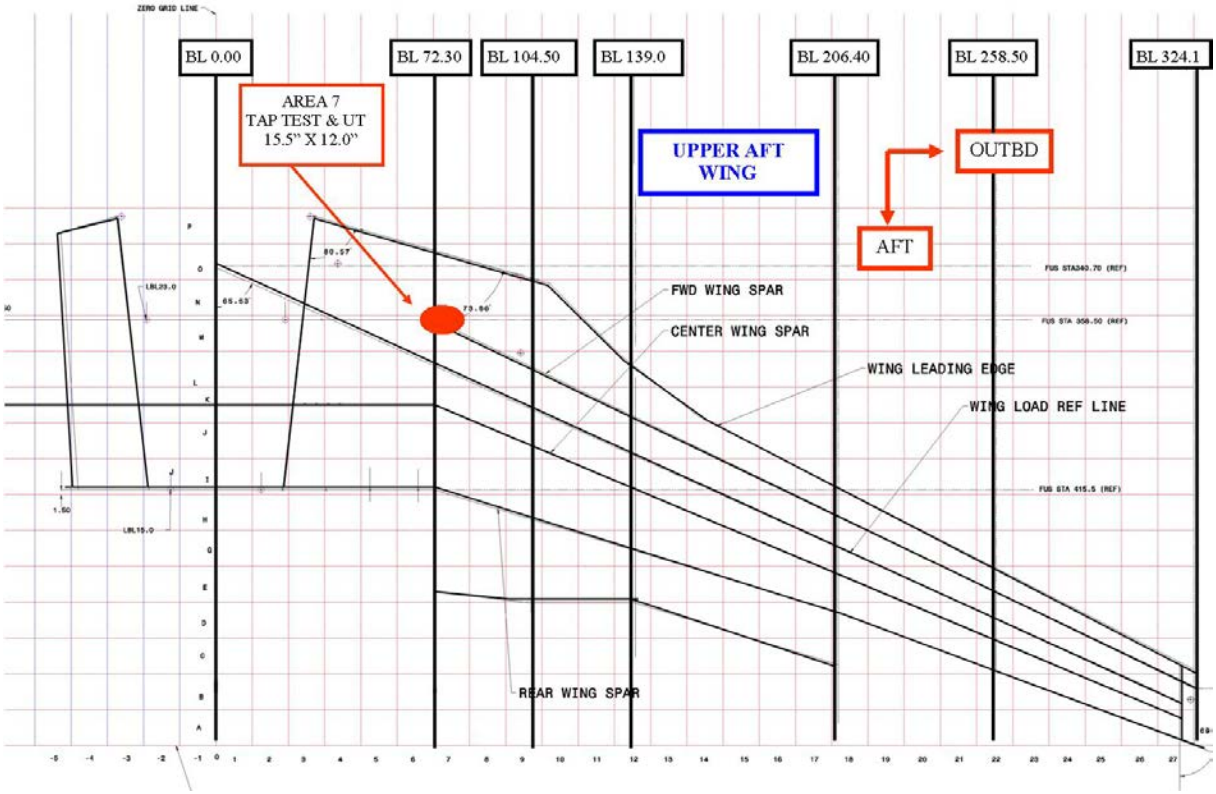

Figure 30. Overview of the right upper aft wing of the Starship

The initial TT examination of the lower aft wing skin revealed disbond in five locations. These areas were inspected with the backup UT procedure for verification. However, only three areas were confirmed with the UT inspection. All areas were re-inspected during the subsequent routine inspection. Another area was discovered during the UT inspection; however, because of its location, TT could not be performed effectively because of accessibility issues. An overview of all defected areas of the right lower aft wing is shown in figure 31. These delaminations were located in the area where the wing was cut away from the test section.

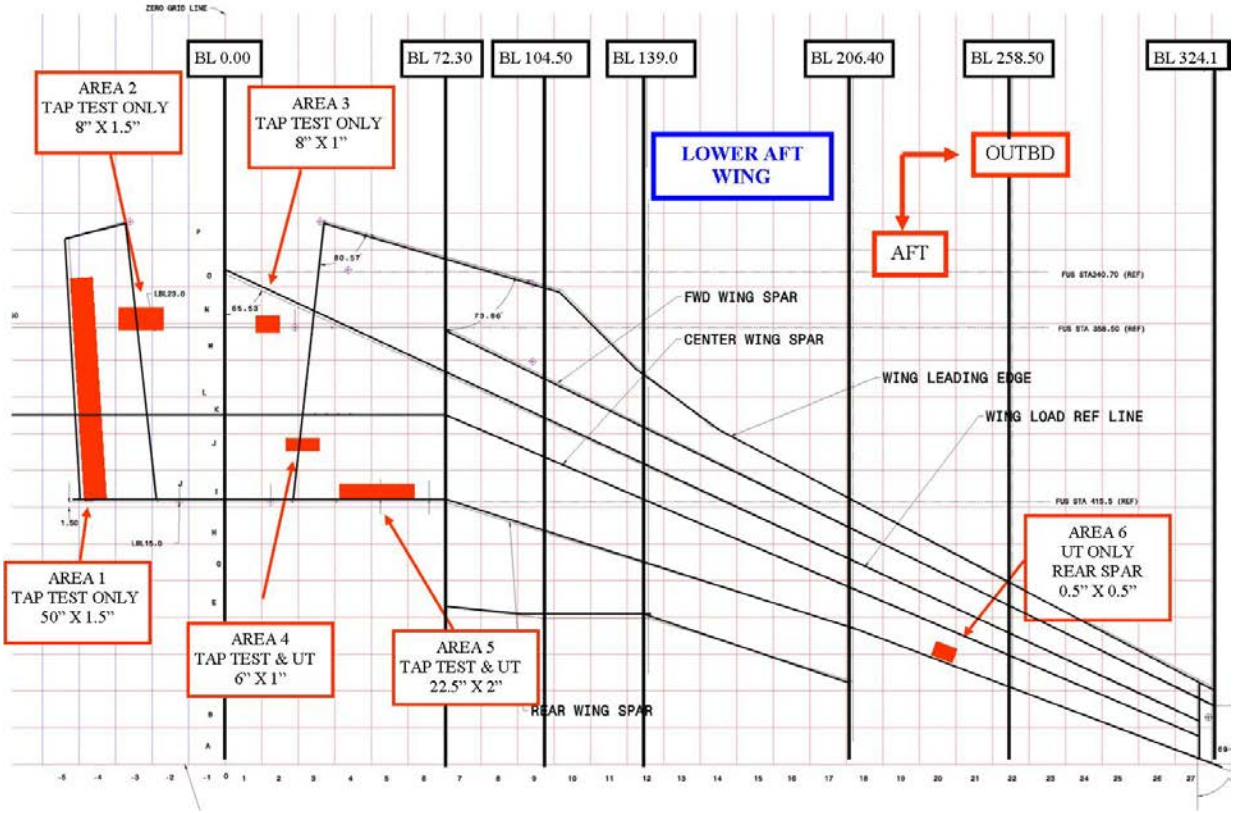

Figure 31. Overview of the right lower aft wing of the Starship

The damaged area identified in the right US was repaired using a wet lay-up bonded to the existing parent structure. The facesheet in the damaged area was removed and scarf sanded using a 0.5″ scarf overlap, as shown in figure 32(a). The repair stacking sequence was PW45/T0/8HS0/T0/8HS90/T0/PW45. The wet lay-up used EA956 laminating resin and was cured at room temperature. The wet lay-up repair ply application is shown in figure 32(b–d). The repair was then vacuum-bagged and cured at room temperature.

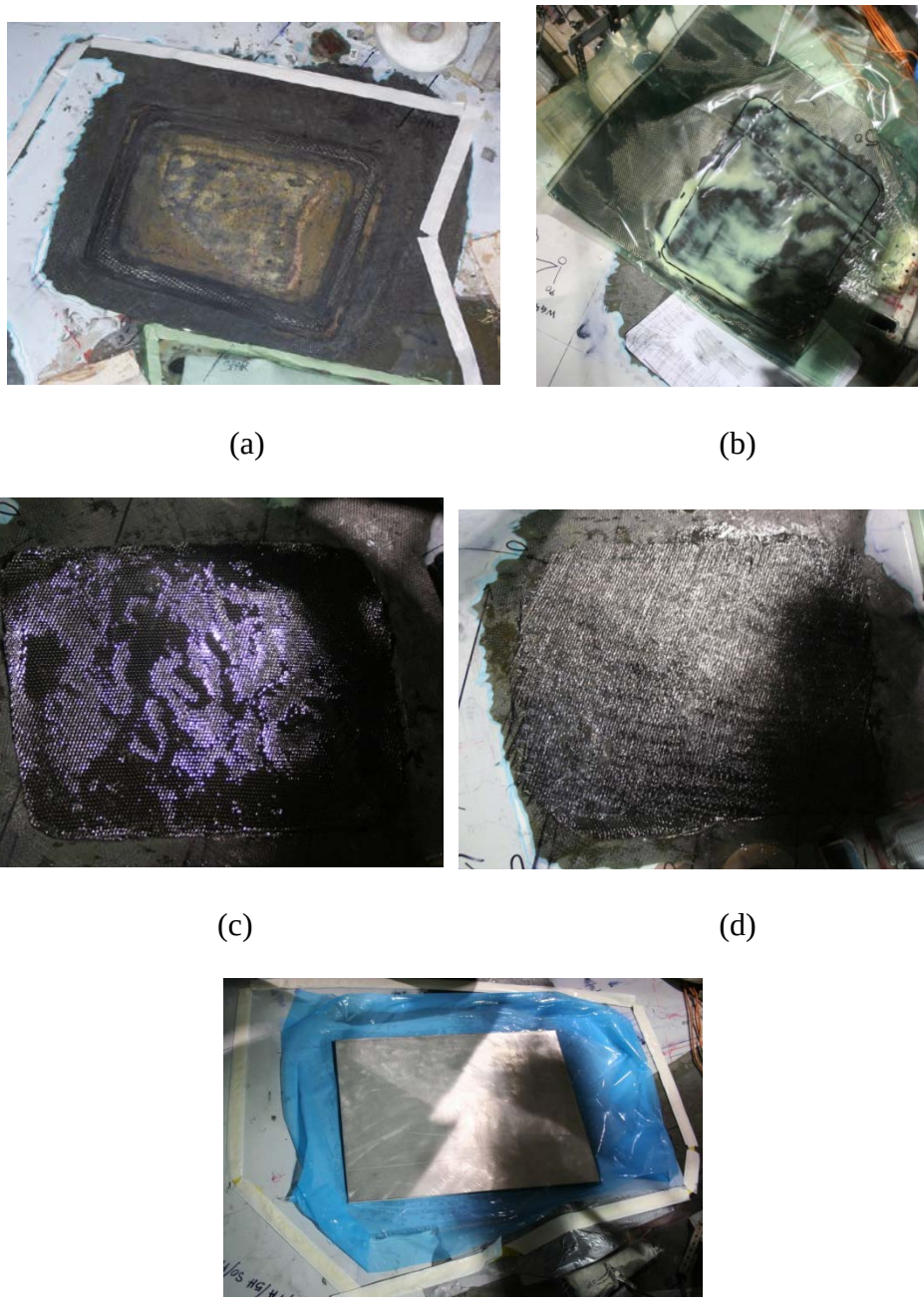

(a) (b)

(c) (d)

(e)

Figure 32. Aft wing repair of US area 7 damage

2.9.2 Starship Aft Wing Full-Scale Test

A full-scale test was conducted at NIAR ASTEC to evaluate the durability of the aft wing. The full-scale test setup is shown in figure 33.

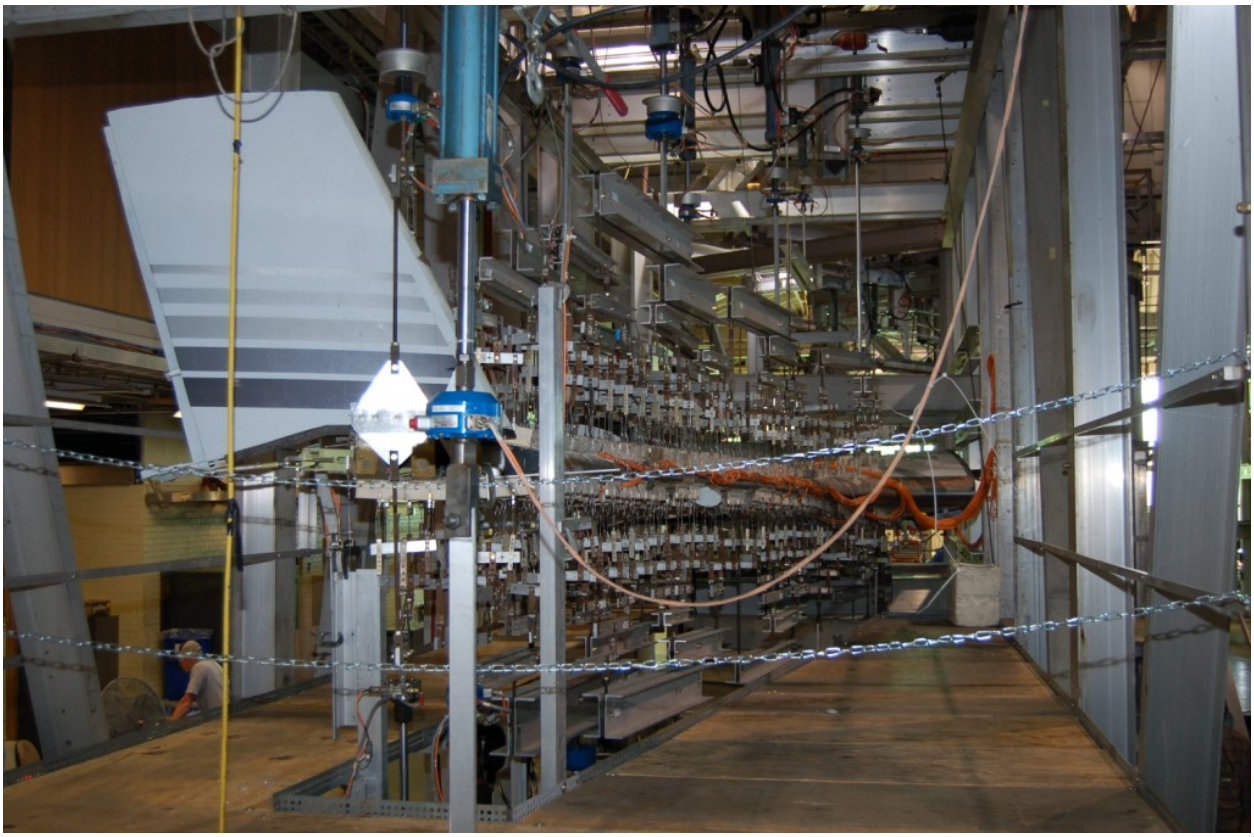

Figure 33. Full-scale test setup

The load case chosen for the full-scale test was the maximum positive moment, which was the most critical load case, because the wing suffered damage during certification testing before sustaining ultimate load. This load case was the most severe in terms of magnitude (maximum moment) applied to the wing's US. The shear/moment and torque introduced closely matched the values that were achieved during the certification test (maximum positive bending condition applied during certification) from RBL 100 to RBL 360; therefore, the test section of interest was the outboard of RBL 100. A plot of the moment diagram as a function of load station location (LSTA) along the load reference axis is shown in figure 34.

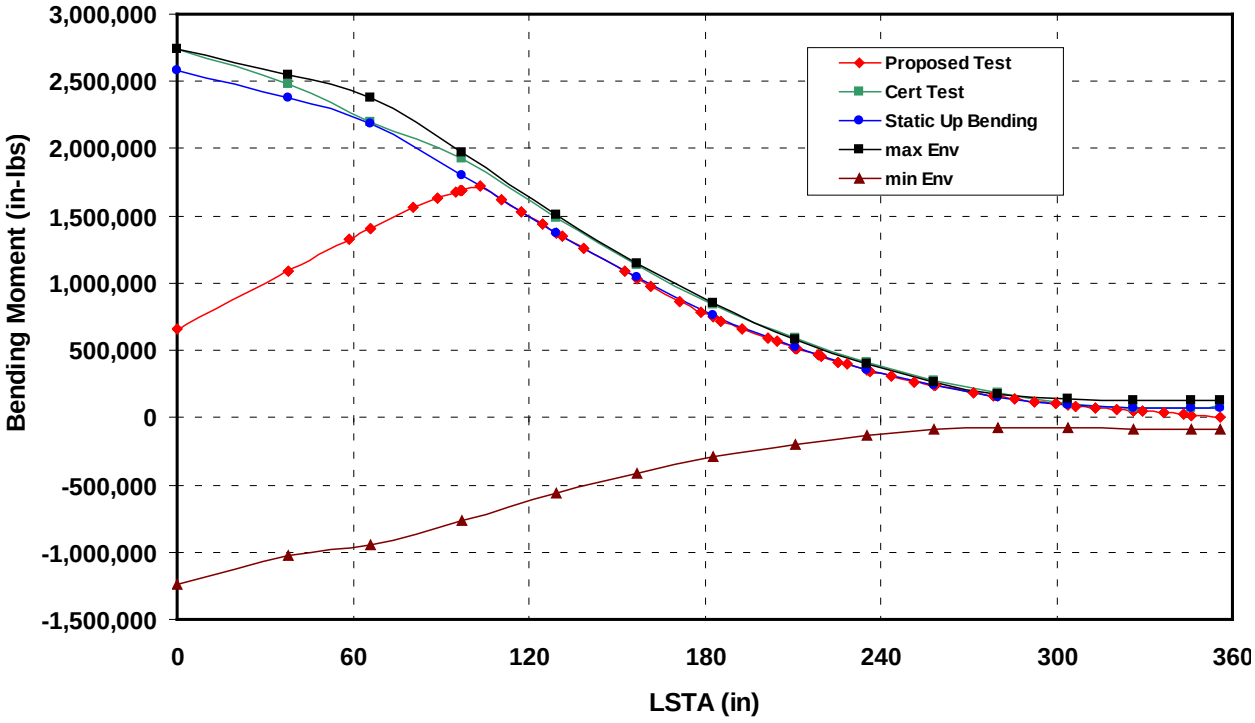

Figure 34. Bending moment vs. LSTA

The full-scale test article was instrumented using strain gages and deflection transducers to monitor deformation during the test. Strain gage locations were based on the analysis conducted during certification used to identify the wing critical stress and strain areas. The locations chosen were the same as those used for the certification test article and are defined in figure 35. The intent was to be able to compare the displacements and strains of the production article with service history to those of the certification test article. The wing was loaded up to 100% limit load with a 10% load increment. Strain gages locations are shown in figure 35. Load, strain, and displacement data were acquired during the test. The deformed wing at limit loads of 40%, 70%, and 100% are shown in figures 36, 37, and 38, respectively.

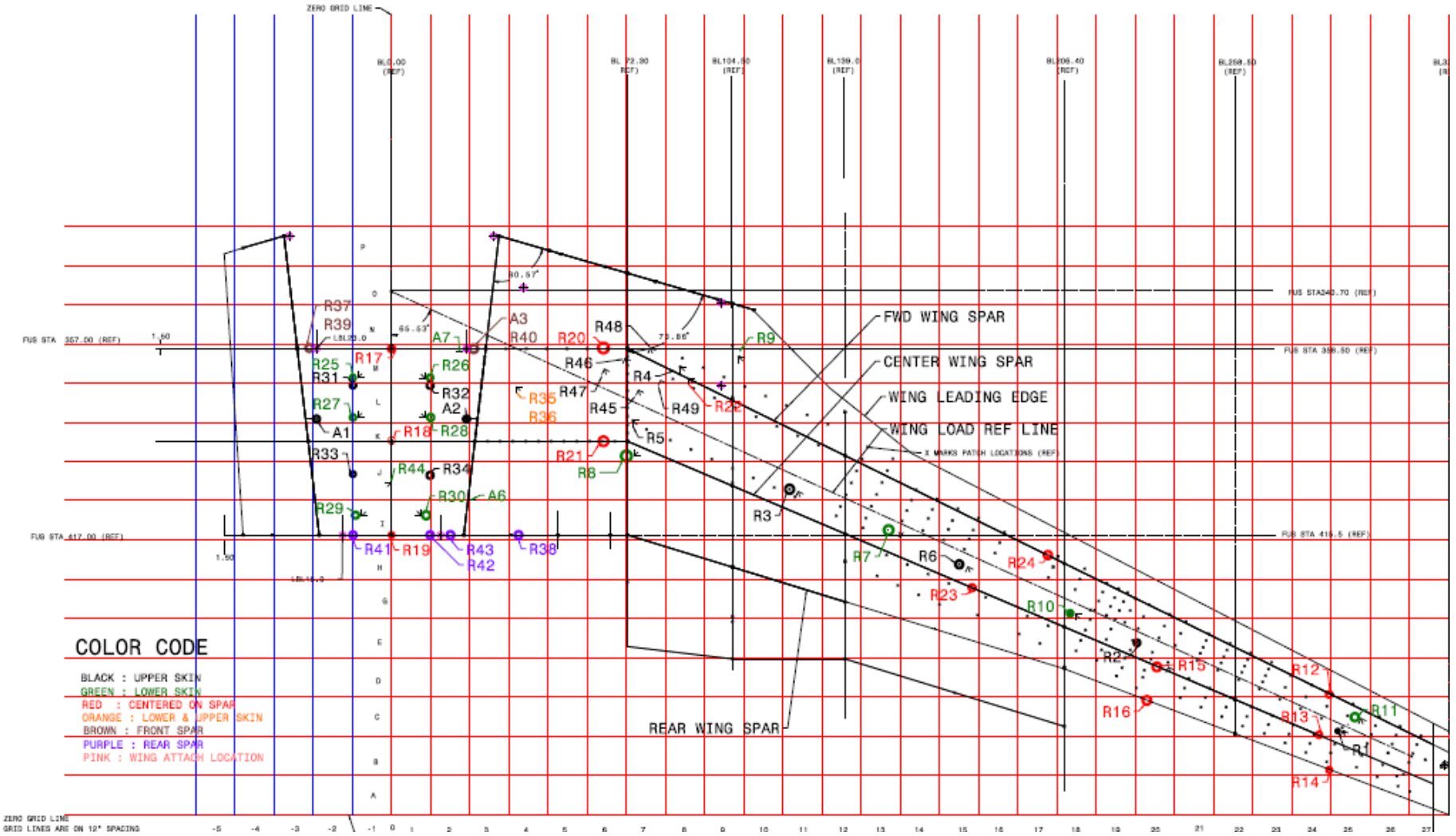

Figure 35. Starship right main wing strain gage identification and NDI inspection grid (12″ spacing between gridlines)

Figure 36. Deformed wing at 40% limit load

Figure 37. Deformed wing at 70% limit load

Figure 38. Deformed wing at 100% limit load

A percent limit load (% LL) versus strain comparison between wing max up-bending certification test (referred to as Limit_Cert), first limit load test conducted (referred to as Limit_Current), and limit load conducted after one lifetime of fatigue (referred to as Limit_Fatigue) are shown in figures 39 and 40 for strain gages R6A (compression, US) and R10 (tension, LS) defined in figure 35. As shown in both figures, strain data from the aged test article correlate well with strain data from the certification article subjected to the same load case. This demonstrates that there is no major change in the overall structure stiffness and structural response.

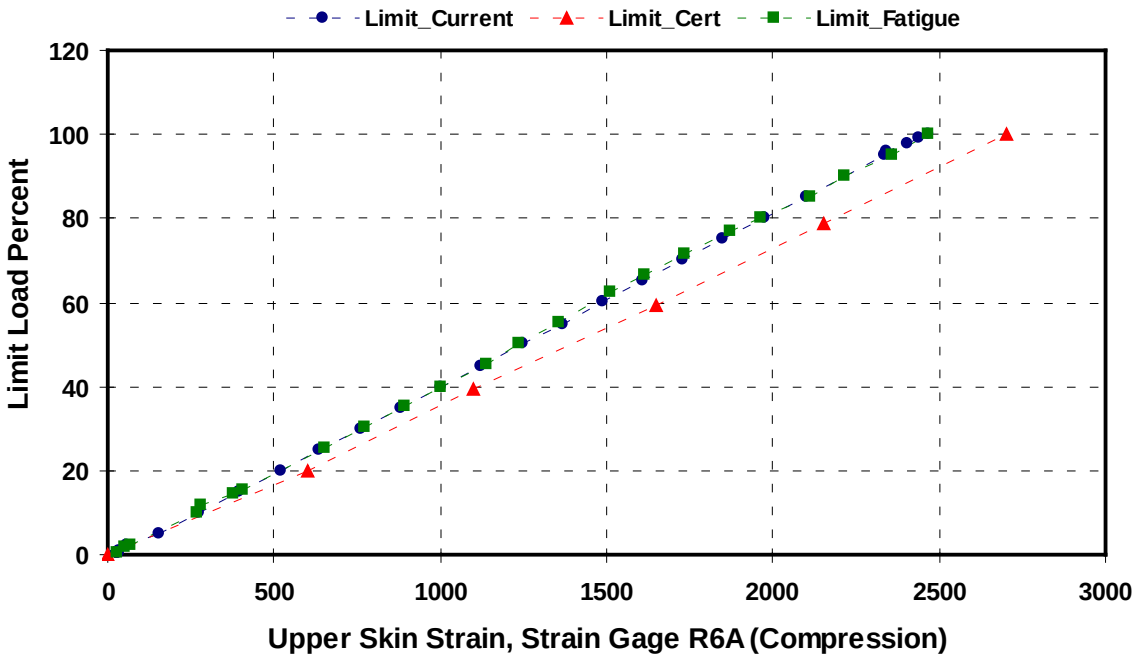

Figure 39. Limit load percent vs. upper wing skin strain comparison (certification vs. post-teardown full-scale tests)

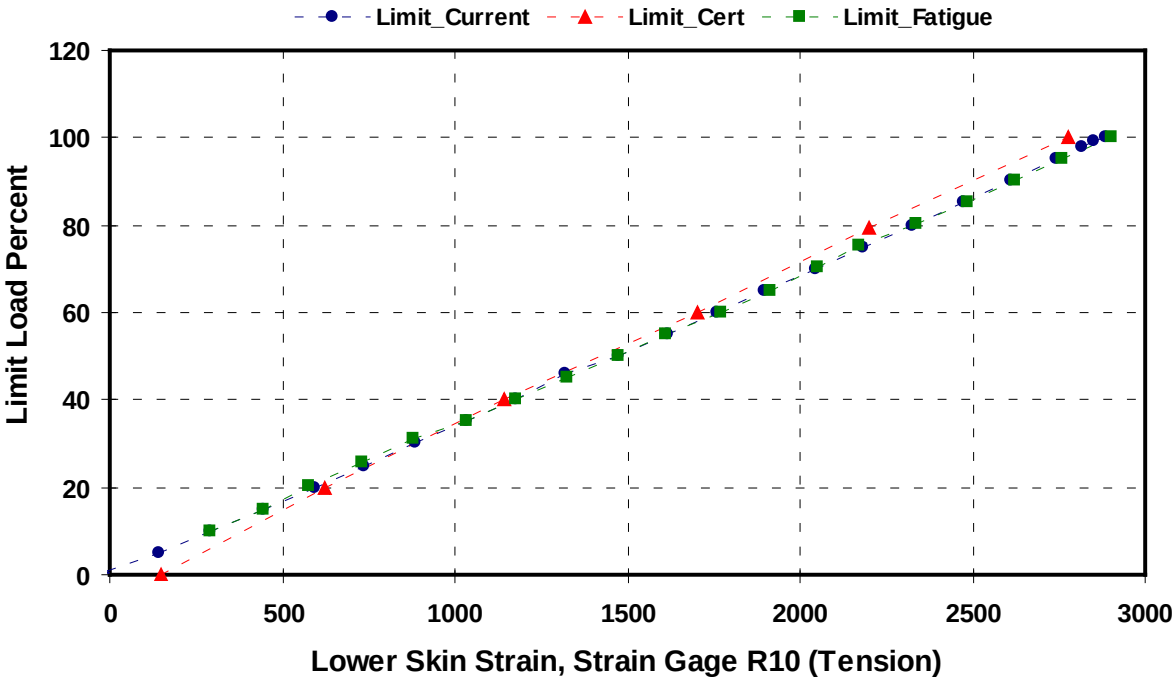

Figure 40. Limit load percent vs. lower wing skin strain comparison (certification vs. post-teardown full-scale tests)

After completing the full-scale limit load test, the aft wing was subjected to an entire fatigue lifetime to investigate the durability of the aged wing. The fatigue loads applied were the same as those developed for the full-scale certification article and included gust, maneuver, landing, and taxi loads. All fatigue loads were applied with a 15% load enhancement factor. Landing loads were not included because the structure did not have landing gear or engines attached. Relieving loads were added to the landing gear and the engine mount fittings to reduce the bending moment at the root of the wing (wing box).

Because of wing fixturing (cantilever wing), negative loads (US tension loads) were truncated and only positive loads (US compression) were applied. The wing was subjected to 200,395 cycles of fatigue, which is equivalent to one lifetime or 20,000 service hours. The spectrum loading sequence is shown in figure 41.

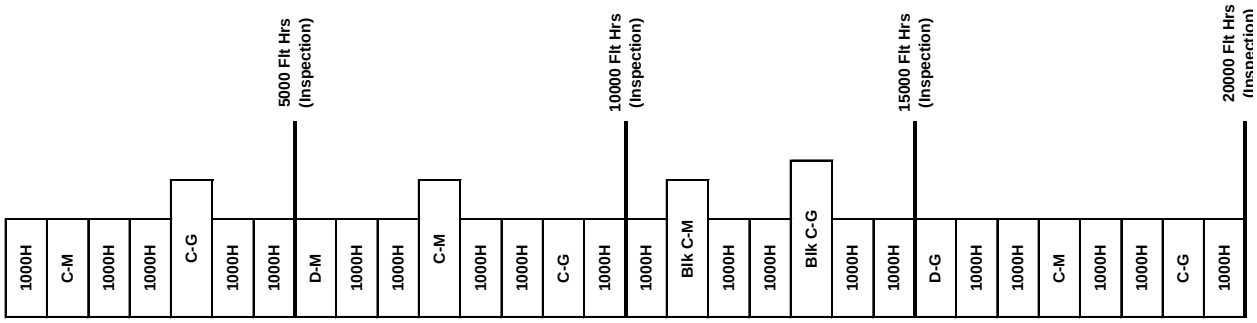

Figure 41. Spectrum loading sequence

After completion of the durability test, the aft wing was inspected and subjected to a limit load residual strength test. The wing sustained a 100% limit positive up-bending test, and residual strength data correlated well with certification data, demonstrating no detrimental aging effects on the structural integrity of the article.

3. CONCLUSIONS

The Starship main wing teardown evaluation showed that the structure, after 12 years of service, held up as well, with no detrimental signs of aging to the naked eye, as would a metal structure with a similar service history.

Thermal analysis results showed no evidence of degradation in the thermal properties of the material, and that the skins were fully cured/cross-linked. Physical tests showed moisture levels indicative of a structure that had reached moisture equilibrium (consistent with other long-term service exposure data published in the literature). Physical test results showed porosity levels higher than 2%, which correlate with original equipment manufacturer production information.

Nondestructive inspection of the left showed no major defects/damage in the skins introduced during manufacture or service. Full-scale test results of the aged wing correlated well with the results obtained for the certification article. There was no indication of fatigue damage, but the 1800 flight hours (≈10% of designed life) was an insufficient amount of time for evaluation.

4. REFERENCES

1. Bleck, M.E., “Starship History,” Beech Aircraft Corporation.

2. *Starship Structural Repair Manual*: *Model 2000 NC-4 and After*, Commercial Publications, Beech Aircraft Corporation, Wichita, Kansas, 1994.

3. Wong, R. and Abbott, R., “Durability and Damage Tolerance of Graphite-Epoxy Honeycomb Structures,” *35th International SAMPE Symposium*, Anaheim, California, April 2–5, 1990.

4. Abbott, R., “Design and Certification of the All-Composite Airframe,” SAE paper 892210, 1989.

5. Wong, R., “Development and Certification of a Composite Airframe,” Society of Manufacturing Engineers, Dearborn, Michigan, 1991.

6. Kolarik, A.L., “Analysis and Certification of the Starship All-Composite Airframe,” SAE paper 900997, 1990.

7. Wong, R., “Sandwich Construction in the Starship,” *37th International SAMPE Symposium*, Anaheim, California, March 9–12, 1992.

8. Aniversario, R.B., Harvey, S.T., McCarty, J.E., et al., “Design, Ancillary Testing, Analysis, and Fabrication Data for the Advanced Composite Stabilizer for Boeing 737 Aircraft,” NASA Contractor Report 3648, April 1983.